Geophys. J. Int. (1998) **135,** 1060–1084

On the nature of regional seismic phases—III. The influence of crustal heterogeneity on the wavefield for subduction earthquakes: the 1985 Michoacan and 1995 Copala, Guerrero, Mexico earthquakes

T. Furumura* and B. L. N. Kennett

Research School of Earth Sciences, Australian National University, Canberra ACT 0200, *Australia*

Accepted 1998 August 5. Received 1998 August 3; in original form 1998 March 3

SUMMARY

The most prominent feature of the regional seismic wavefield from about 150 to over 1000 km is usually the *Lg* phase. This arrival represents trapped *S*-wave propagation within the crust as a superposition of multiple reflections, and its amplitude is quite sensitive to the lateral variation in the crust along a propagation path. In an environment where the events occur in a subduction zone, such as the western coast of Mexico, quite complex influences on the character of the regional wavefield arise from the presence of the subduction zone.

The great 1985 Michoacan earthquake ($M_W = 8.1$), which occurred in the Mexican subduction zone, was one of the most destructive earthquakes in modern history and its notable character was that at Mexico City, located over 350 km from the epicentre, there was strong ground shaking almost comparable to that in the epicentral region that lasted for several minutes. Considerable effort has been expended to explain the origin of the unusual observed waves that caused the severe damage in the capital city during the destructive earthquake.

The nature of the propagation process in this region can be understood in part by using the detailed strong-motion records from the 1995 Copala, Guerrero ($M_W = 7.4$) earthquake near the coast to the south of Mexico City, which also had an enhanced amplitude in the Valley of Mexico.

Numerical modelling of both *P* and *S* seismic waves in 2-D and 3-D heterogeneous crustal models for western Mexico using the pseudospectral method provides direct insight into the nature of the propagation processes through the use of sequences of snapshots of the wavefield and synthetic seismograms at the surface. A comparison of different models allows the influences of different aspects of the structure to be isolated.

2-D and 3-D modelling of the 1985 Michoacan and 1995 Copala earthquakes clearly demonstrates that the origin of the long duration of strong ground shaking comes from the *Sn* and *Lg* wave trains. These *S*-wave arrivals are produced efficiently from shallow subduction earthquakes and are strongly enhanced during their propagation within the laterally heterogeneous waveguide produced by the subduction of the Cocos Plate beneath the Mexican mainland. The amplitude and duration of the *Lg* coda is also strongly reinforced by transmission through the Mexican Volcanic Belt from the amplification of *S* waves in the low-velocity surficial layer associated with *S*-to-*P* conversions in the volcanic zone.

The further amplification of the large and long *Lg* wave train impinging on the shallow structure in the basin of Mexico City, with very soft soil underlain by nearly rigid bedrock with a strong impedance contrast, gives rise to the destructive strong ground shaking from the Mexican subduction earthquakes.

Key words: 1985 Michoacan earthquake, 1995 Copala Guerrero earthquake, *Lg* wave, pseudospectral method, subduction zone, wave propagation.

* Present address: Hokkaido University of Education, Midorigaoka 2-34-1, Iwamizawa, 068-8642, Japan. E-mail: furumura@iwa.kokkyodai.ac.jp

GJI000 16/11/98 13:22:19 3B2 version 5.20
The Charlesworth Group, Huddersfield 01484 517077

1 INTRODUCTION

The dominant seismic phases at regional distances are usually the crustal *Pg* and *Lg* phases representing trapped *P*- and *S*-wave energy within the crustal waveguide. In particular, the *Lg* phase propagating on continental paths at regional distances, from about 150 to 1000 km, generally shows very large amplitude, with wave trains of long duration. Since the excitation of the *Lg* phase is relatively insensitive to the details of the source mechanism and the source depth in the crust, *Lg* has long been utilized for a robust ($M_{\rm Lg}$) magnitude estimation (e.g. Nuttli 1988) as well as in nuclear discrimination studies (see e.g. Pomeroy *et al.* 1982; Blandford 1996).

The *Lg* phase can be regarded either as a superposition of multiply reflected *S* waves in the crust or as a sum of a number of higher-mode surface waves sampling from the free surface to the crust–mantle boundary. The details of the nature of the *Lg* wave train arise from complex interference effects and are very sensitive to lateral change in the crustal structure compared with other mantle *Pn* and *Sn* phases, crustal *Pg* waves and fundamental Rayleigh *Rg* waves (e.g. Kennett 1989). The sensitivity of the character of *Lg* to crustal properties has often been used to estimate material parameters such as the velocity gradient at the base of the crust (e.g. Bowman & Kennett 1991) and attenuation factors (e.g. Campillo 1987; Yamamoto *et al.* 1997). In the presence of sharp lateral crustal variations, *Lg*-wave transmission can be blocked (e.g. Gregersen 1984; Kennett & Mykkeltveit 1984; Baumgardt 1990; Gibson & Campillo 1994). In a companion paper, Paper II (Furumura & Kennett 1997), we simulated the character of *Lg*-wave propagation in laterally heterogeneous crustal models and demonstrated how the *S*-wave energy is extracted from the crustal waveguide in the presence of strong lateral variations. For example, the near extinction of *Lg* crossing the Matezone in the North Sea Central Graben is associated with *Lg*-to-*P* conversions due to the presence of a thick sedimentary layer and significant elevation in the Moho beneath the graben with transfer of energy to *Sn*.

Such studies on *Lg*-wave propagation in heterogeneous crust clearly indicate that both small- and large-scale variations that alter the lateral velocity gradients in the crustal waveguide can severely affect the character and attenuation of the *Lg* wave.

The great 1985 Michoacan earthquake ($M_W = 8.1$), which occurred on a segment of the plate boundary along the Mexican subduction zone, was the most damaging in Mexico City in modern history. The event caused more than 10 000 casualties in the capital city. A notable feature of the strong ground shaking from this devastating earthquake was that severe ground shaking, almost comparable to that in the epicentral zone, lasted for more than 3 minutes in the lake-bed zone of Mexico City, even though this lies about 350–400 km away from the epicentre (see e.g. Anderson *et al.* 1986).

Considerable attention has been directed towards the nature of the unusually large, long-duration ground shaking in Mexico City. A number of simulations have been made of the seismic response in the basin of Mexico City (e.g. Bard *et al.* 1988; Sánchez-Sesma *et al.* 1988; Kawase & Aki 1989; Mateos *et al.* 1993a,b; Chávez-García & Bard 1993a,b; Bard & Chávez-García 1993). It is clear that strong amplification of the ground shaking from the earthquake arises from the presence of highly compressible saturated clays, which form the lake-bed zone in the basin of Mexico City, and the strong impedance contrast with the bedrock beneath. However, such simulation results, in which only the seismic amplification in the basin is taken into account, fail to provide a satisfactory explanation of the unusually long ground oscillations unless rather unrealistic physical parameters are employed in the simulation, such as neglecting the anelastic attenuation effect ($Q = \infty$) (Kawase & Aki 1989) or employing a strong fluctuation in basin-bottom topography (Bard *et al.* 1988) or random variations in the thickness of the surficial clay layer in the lake-bed zone (Chávez-García & Bard 1994). Although alternative explanations for the strong ground shaking in the lake-bed zone have been proposed, such as the influence of the lateral resonance of horizontally propagating *P* waves in the clay layer (Flores *et al.* 1987; Seligman *et al.* 1989; Mateos *et al.* 1993a,b) and a gravity wave generated in soft soil from strong ground shaking (Lomnitz 1990; Chávez-García & Bard 1993a,b; 1995), such mechanisms are very unlikely to have affected the ground motion in Mexico City during the damaging earthquakes (Lomnitz 1995; Sánchez-Sesma & Luzón 1996).

Another explanation proposed for the origin of the long ground shaking in Mexico City is that the incident wave on the lake-bed zone had already acquired a long duration as a result of multipathing and scattering of waves during the long propagation path (Singh & Ordaz 1993). This hypothesis is strongly supported by a number of recent studies based on wave-propagation simulation and the analysis of seismic records from the broad-band stations that have recently been widely installed in Mexico. For instance, Campillo *et al.* (1988, 1989) identified the *Lg* wave in synthetic seismograms for *SH*-wave propagation in a shield crustal structure. Fäh *et al.* (1994) used a hybrid technique that combined a modal-summation method for simulating a seismic wave propagating through a 1-D shield zone with a 2-D finite difference method to evaluate the seismic wave disturbances for the heterogeneity in the basin of Mexico City. They concluded that the dispersion of high-frequency surface waves during the relatively long propagation path was the main cause of the long duration of the incident signal impinging on the basin. Chávez-García *et al.* (1995) analysed the surface-wave propagation character in Mexico using data from a number of broad-band stations and showed that the seismic energy in the period range 3–10 s is carried by Rayleigh and Love modes from the Mexican coast to Mexico City with an additional surface wave generated by lateral heterogeneity in the crust. Barker *et al.* (1996) analysed the principal direction of later phase arrivals from dense array records, which suggest that the long *S*-wave coda results from scattering and multipathing from the boundaries of the Mexican Volcanic Belt (MVB) surrounding Mexico City. Shapiro *et al.* (1997) conducted 2-D simulations of observed records propagating through the MVB and concluded that the anomalously low shear-wave velocity of the volcanic rocks significantly increases the amplitude and signal duration because of dispersion of the surface waves.

The objectives of this study are two-fold: first to extend our previous study (Part II; Furumura & Kennett 1997) on the nature of the regional phases in laterally heterogeneous crustal waveguides to include the effects of subduction zone earthquakes; and second to understand the generation mechanism of the anomalously large and long-duration ground shaking during the long propagation paths from the great Mexican earthquakes. We will simulate both *P* and *S* wavefields for a

GJI000 16/11/98 13:22:47 3B2 version 5.20
The Charlesworth Group, Huddersfield 01484 517077

variety of 2-D and 3-D crustal models by using the pseudo-spectral method for 2-D *P–SV* waves (Furumura & Takenaka 1996) and a 3-D wave code (Furumura *et al.* 1996) in order to investigate the relative importance of different aspects of crustal heterogeneity on the character of the seismic wavefield.

We use recent three-component seismograms of the 1995 Copala, Guerrero, Mexico earthquake ($M_W = 7.4$) recorded on the strong ground motion network to provide a basis for understanding the character of the regional wavefield in Mexico. We examine the differences in the character of regional phases for two different reference models, (1) a stratified shield crustal model and (2) a simple subduction model including the descent of the Cocos Plate beneath the Mexican mainland using 2-D wavefield calculations. These reference models are then combined with different styles of crustal heterogeneity such as near-surface topography with a low-velocity surficial layer and velocity gradients in the lower crust. We examine the relative importance of these crustal variations in modifying the nature of the regional phases for various source depths and wave types, and in particular look at the enhancement of wave amplitude in the Valley of Mexico. Finally, we simulate wave propagation in three dimensions for the 1995 Copala, Guerrero and 1985 Michoacan earthquakes in order to complement the 2-D simulation results and to gain further insight into the nature of complex wave propagation in realistic 3-D heterogeneous structures.

2 OBSERVATION OF SEISMIC WAVE PROPAGATION FROM THE MEXICAN SUBDUCTION EARTHQUAKES

The Cocos Plate dips under the western coast of Mexico with a relatively shallow subduction angle of about 10–15° towards the NE beneath the North American Plate (see e.g Suárez *et al.* 1990; Singh & Pardo 1993). This subduction zone has been associated with a number of huge earthquakes in recent years, of which the largest was the Michoacan earthquake of 1985 September 19 ($M_W = 8.1$). This event led to a significant amount of damage in Mexico City, even though it is located 350–400 km from the epicentre (see e.g. Anderson *et al.* 1986).

A dense network of strong ground motion recorders was installed in the Mexican mainland just after the devastating earthquake, both to understand the character of the wavefield and to investigate the cause of the strong ground shaking in the capital city (e.g. Anderson & Quaas 1988; Quaas *et al.* 1996). On 1995 September 15 an $M_W = 7.4$ earthquake occurred in Copala, Guerrero, Mexico, the largest event since the destructive 1985 earthquake (hereafter we will refer to this event as the 1995 Copala earthquake). The epicentre lay some 300 km to the south of Mexico City. This event had some similarities with the great 1985 event, with a shallower depth of $H = 17$ km, and displacement along the strike of the subduction plate with a shallow thrust low-dip-angle focal mechanism (Sánchez-Sesma *et al.* 1993; Anderson *et al.* 1995).

Fig. 1 shows the location of the strong motion accelerograph network with a projection of hypocentres of the 1985 Michoacan and 1995 Copala earthquakes, and Fig. 2 displays the three-component velocities recorded at those stations with good site conditions (solid and volcanic rocks). The velocity seismograms have been produced by an integration of filtered accelerograms. A band-pass filter with −3 db points at 0.1 and 1 Hz has been applied in order to reduce instrumental noise and to enhance the period range around 2–3 s that caused the severe ground shaking in the basin of Mexico City during the damaging earthquake.

The seismic motions from the earthquake are well recorded at the inland stations, which provide coverage of the regional wavefield along a nearly N–S line from the epicentre to Mexico City with a distance range of 15–335 km. In the seismograms the dominance of the *S* wave in the records of all three components is clearly seen. The records are characterized by arrivals with a wide group velocity range from 3.2 to 2.5 km s^{-1}, which we tentatively correlate with the *Lg* wave train usually seen in continental regions (see e.g. Press & Ewing 1952). In front of the *Lg* wave train there is a distinct onset of *S* energy beyond 120 km, with a group velocity around 3.5 km s^{-1} and a slightly higher phase velocity. This arrival must be associated with *Sn* even though it is somewhat slower than usual. *Sn* and *Lg* are dominant at distances beyond 120 km from the epicentre. The relatively long duration of the *Lg* wave train increases with distance. Beyond 250 km from the epicentre, the amplitude of *Lg* is enhanced and even before the waves impinge on the basin of Mexico City the *S* waves have a large amplitude and a long duration (over 80 s from the onset of the *Sn* arrival to the end of the *Lg*-wave coda).

The very soft sediment below Mexico City will amplify this large and very long input motion to produce very significant ground shaking for major earthquakes. This is clearly demonstrated in the three-component record at a lake-bed station (RMCS—one example out of over 50 of lake-bed stations; Fig. 2a, right panel) in which enhancement of the vertical motion and much greater amplification of the horizontal motion are seen. It is interesting to see in the seismograms that the amplitude of the *Lg* wave is suddenly weakened after travelling through Mexico City; this is very similar to the dramatic loss of *Lg*-wave amplitude after passing through the thick sediments of the North Sea Central Graben zone (Furumura & Kennett 1997).

The dominant seismic *Lg* wave for the inland stations is not seen in records of coastal stations at comparable distances (Fig. 2b). The coastal stations lie close to a node in the *S*-wave pattern. However, the attenuation of the seismic waves is much greater along the coastal path, so that the sensors were not triggered at stations further than 200 km from the epicentre. The rapid drop in *Lg* amplitude along the coast of Mexico is likely to be influenced by the low crustal thickness below the coast ($\sim$20 km). The *S* waves reverberating in the thin crust are rapidly weakened due to geometrical and anelastic attenuation in the crust, and can also leak energy into the subducted plate lying below the crust. This situation is somewhat analogous to the failure of *Lg* to propagate beyond 100 km in oceanic crust (see e.g. Press & Ewing 1952).

Fig. 3 illustrates the pattern of the peak velocities for the three components as a function of epicentral distance for both the inland and the coastal stations. Superimposed on the observations is the empirical attenuation curve for horizontal-component *S* waves with periods around 2 s derived by Ordaz & Singh (1992). In Fig. 3 the increase in peak velocity for inland stations at epicentral distance beyond 200 km and the dramatic drops in value for coastal stations are clearly seen. At a distance of about 300 km, just before Mexico City, the peak amplitude in the *Lg* wave train is roughly 10 times greater

GJI000 16/11/98 13:22:48 3B2 version 5.20
The Charlesworth Group, Huddersfield 01484 517077

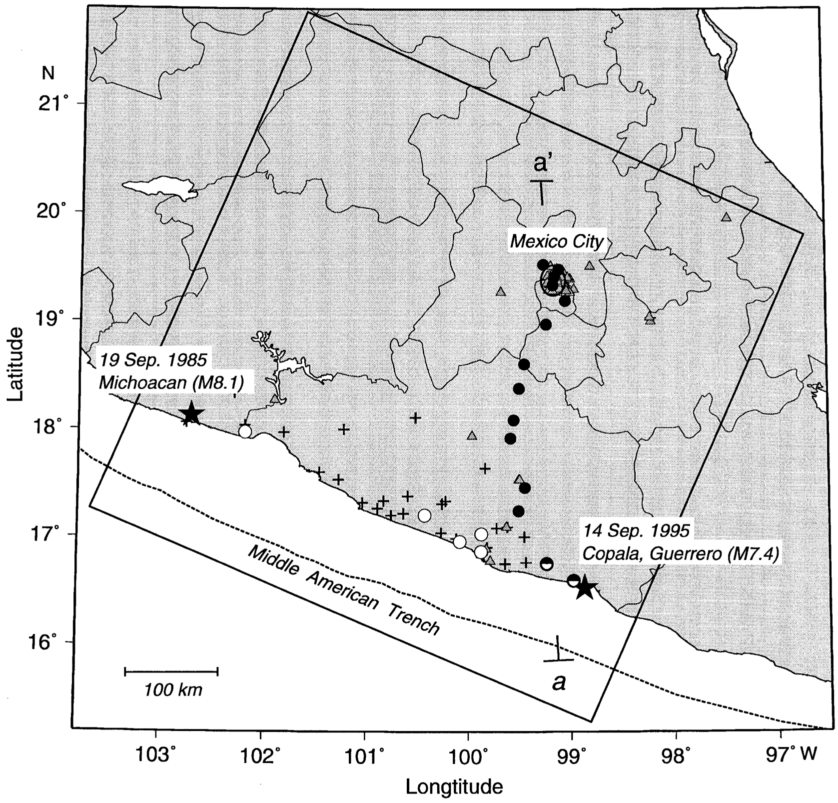

Figure 1. Map of Mexico showing the hypocentres of the 1985 Michoacan and 1995 Copala, Guerrero earthquakes and the locations of the strong-ground-motion stations. Solid circles denote the inland stations and open circles mark the coastal stations that are used in this study. Triangles denote those stations whose data is not used in the analysis. Crosses indicate the stations where strong-motion data were not obtained during the 1995 Copala earthquake. The mark a–a′ and the square indicate the zones used for 2-D and 3-D simulations.

than that suggested from the relation of Ordaz & Singh (1992). Such an amplification anomaly in some inland stations near Mexico City has already been noted by Ordaz & Singh (1992) and Singh *et al.* (1995) for all shallow-depth ($H < 35$ km) coastal earthquakes within a 0.2–2 Hz frequency range.

We can explain these results as arising from the dominance of the *Lg* wave at regional distances for the inland stations. We note that *Lg* has a large amplitude from shallow earthquakes in the crust and that the power of the *Lg* wave is generally largest in the frequency range 0.1–5 Hz (see e.g. Herrmann & Kijko 1983). As we shall demonstrate from numerical modelling, the influence of the subduction zone is also important: the amplitude pattern seen in Fig. 3 is much more complicated than those usually seen for continental paths (see e.g. Kennett 1993).

3 SEISMIC WAVE PROPAGATION SIMULATION FOR MEXICO

We simulate the character of the regional seismic wavefield by using the pseudospectral method for 2-D *P–SV* waves and including anelasticity (Furumura & Takenaka 1996). The pseudospectral method (e.g. Kosloff *et al.* 1984; Reshef *et al.* 1988) is an attractive alternative method to the finite difference scheme for the modelling of seismic wave propagation in heterogeneous media. In the pseudospectral method, the field quantities are expanded in terms of Fourier interpolation polynomials, and the spatial differentiation of the equations is analytically performed in the wavenumber domain, thus only two gridpoints per wavelength are theoretically sufficient to model the wave propagation. Therefore, this approach to numerical modelling offers high-accuracy results with a reduction of several orders of magnitude in both computational time and memory requirements compared with the traditional finite difference schemes (see e.g. Fornberg 1987; Daudt *et al.* 1989) and is very efficient for large-scale modelling.

Our aim is to examine the character of the observations for the 1995 Copala earthquake and the way in which the features of the wavefield relate to the structure. We therefore employ a number of different 2-D models.

As an initial example, we compare the propagation of regional seismic phases in (1) a shield structure and (2) a simple model including the Mexican subduction zone, in order to see the character and evolution of regional phases with distance from the source. The subduction of the Cocos Plate is almost parallel to the coast of Mexico, so we are able to use a 2-D model along the line a–a′ perpendicular to the trench (Fig. 1), as a good approximation to the actual situation.

The shield reference model is similar to those employed in previous simulations of wave propagation in Mexico (e.g. Campillo *et al.* 1988, 1989; Fäh *et al.* 1994). The model, which includes a sharp velocity jump at a Conrad discontinuity (17 km depth) and a relatively deep Moho at 46 km depth, is illustrated in Fig. 4. This crustal model for Mexico is of continental type, but is somewhat different from northwestern

GJI000 16/11/98 13:22:50 3B2 version 5.20
The Charlesworth Group, Huddersfield 01484 517077

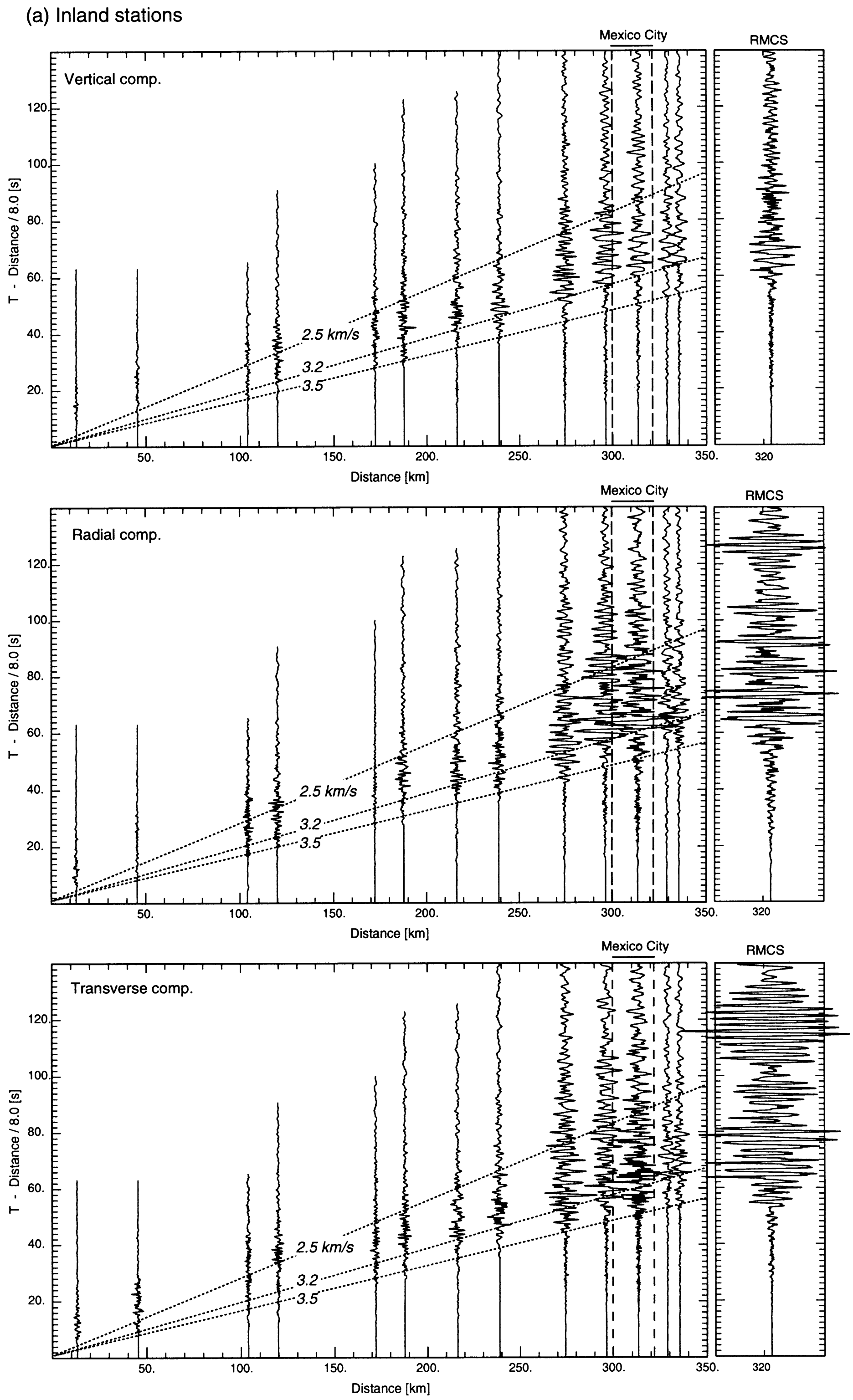

Figure 2. Observed three-component velocity seismograms for vertical (top panel), radial (middle panel) and transverse components (bottom panel) recorded at the stations illustrated in Fig. 1 during the 1995 September 15 ($M_W = 7.4$) event. A bandpass filter from 0.1 to 1 Hz is applied. The location of Mexico City is marked in the figure. (a) Seismic record at inland stations and a lake-bed station in Mexico city (RMCS, right); (b) coastal stations (note that amplitude is multiplied by a factor of two). Lines of constant group velocities of 3.5, 3.2 and 2.5 km s^{-1} are shown.

Europe (see e.g. Furumura & Kennett 1997, Fig. 1) and the western United States (see e.g. Olsen *et al.* 1983, Fig. 14), both of which display a shallower depth to the Moho of about 30 km and a rather smaller velocity jump at the Conrad discontinuity.

The simple subduction model includes the Cocos Plate descending beneath the Mexican mainland and is based on the work of Valdes *et al.* (1986) derived from an analysis of major reflection experiments and gravity data. The

GJI000 16/11/98 13:22:51 3B2 version 5.20
The Charlesworth Group, Huddersfield 01484 517077

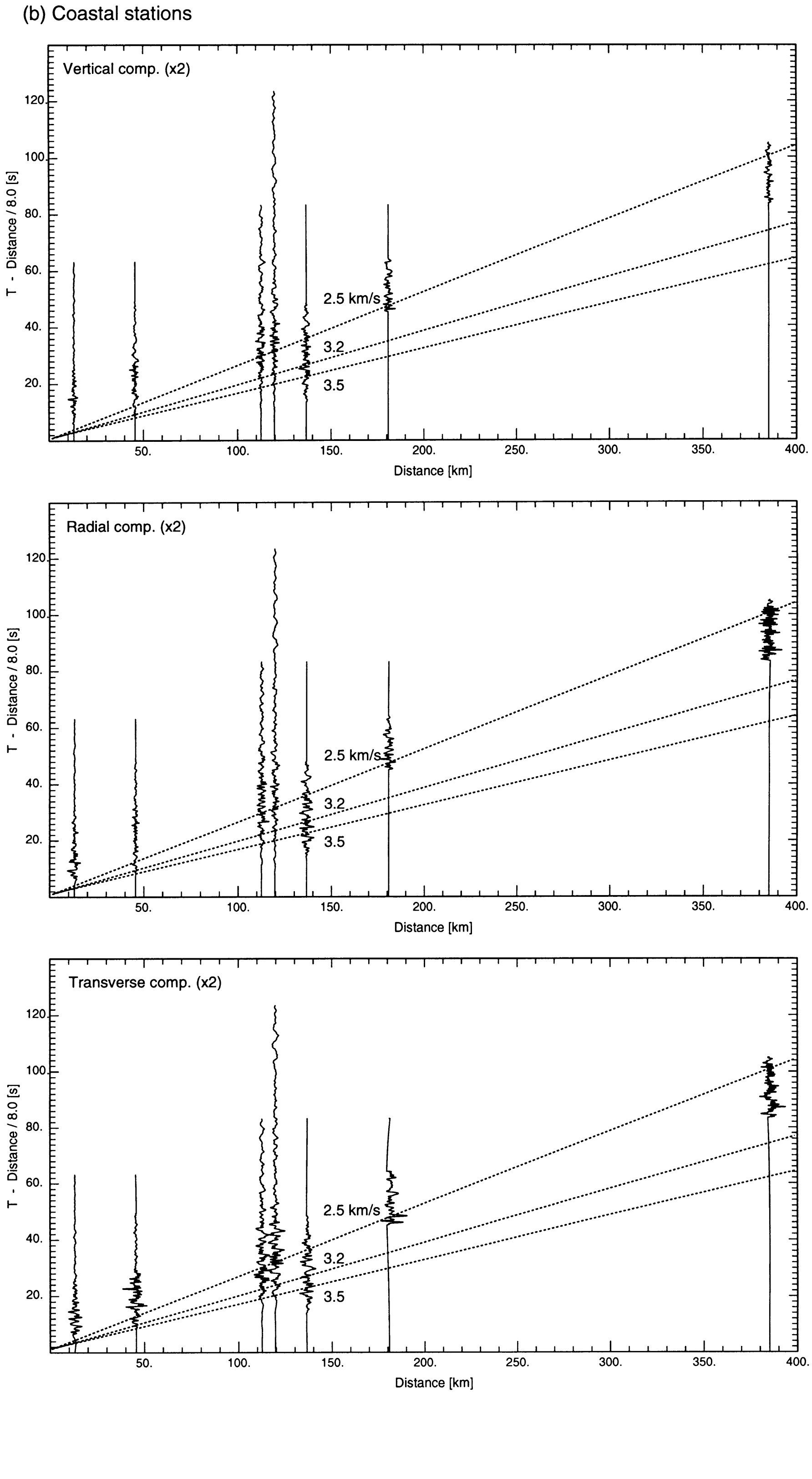

Figure 2. (*Continued.*)

subducting plate consists of two parts: oceanic upper crust and oceanic basalt with low velocities and a combined thickness of 8 km; and high-velocity oceanic lithosphere 20 km thick. We have modelled the *S*-wave velocity for the upper crust and basalt layers with a V_P/V_S ratio of 1.74 and allowed for significant attenuation, $Q=200$. Lower attenuation was imposed ($Q=3000$) for the subducting oceanic lithosphere.

In both of the 2-D models we have included an allowance for surface topography and the variation in near-surface structure. A sedimentary basin 20 km long by 2 km deep representing the subsurface geology below Mexico City is placed just below the free surface 300 km away from the epicentre of the 1985 Copala earthquake. In this basin we use very slow velocities ($V_P=2.0$ km s^{-1}, $V_S=1.0$ km s^{-1})

GJI000 16/11/98 13:22:52 3B2 version 5.20
The Charlesworth Group, Huddersfield 01484 517077

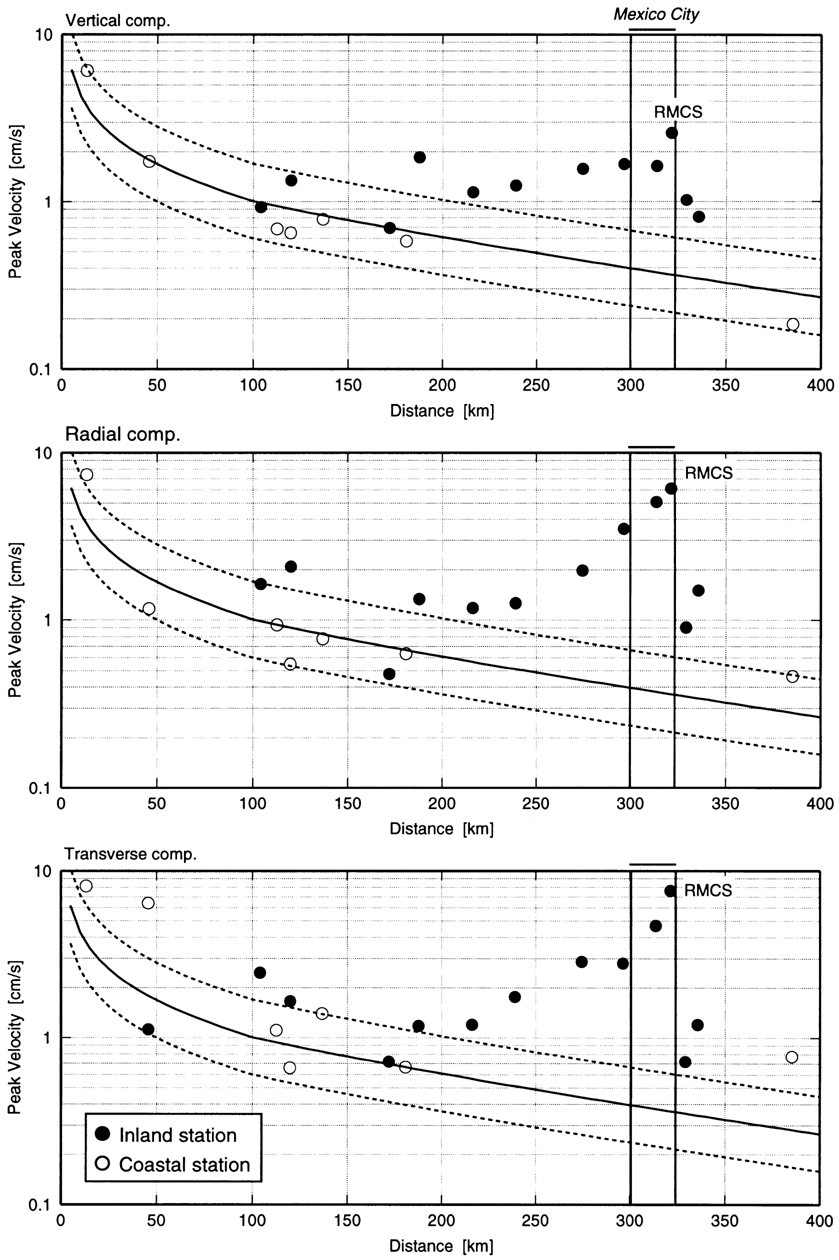

Figure 3. Attenuation of peak amplitude of ground velocity as a function of hypocentral distance for the inland (solid circles) and coastal stations (open circles). Top panel: vertical component; middle panel: radial component; bottom panel: transverse component. The continuous curves represent the empirical relation for S-wave amplitude for frequency around 2 s for Mexican earthquakes deduced by Ordaz & Singh (1992); the dashed curves represent the percentiles 16 and 84.

with high attenuation ($Q=80$), compared with the surrounding crystalline upper crust ($V_P=4.3$ km s^{-1}, $V_S=2.5$ km s^{-1}, $Q=200$).

The numerical model for the 2-D anelastic simulation covers a zone 512 km long by 128 km deep that is discretized using uniform grid intervals of 0.5 km. The influence of grid-edge effects is minimized by introducing an absorbing buffer zone of 20 gridpoints surrounding the discretized region following Cerjan *et al.* (1985). To represent the 1995 Copala event, we have used a seismic double-couple line source representing a low-angle thrust-fault source excited 17 km below the surface. The seismic source has a source time history with a pseudo-delta function that imparts seismic waves with a dominant period around 2 s.

Using the minimum S-wave velocity in the basin ($V_S=1.0$ km s^{-1}) and the minimum S wavelength (2 km) for the source ($T=2$ s), the number of gridpoints per wavelength for this model is 4, which is sufficient for the pseudospectral simulation.

We present a sequence of snapshots for the seismic wavefield with P and SV components separated by calculating the divergence and curl of the displacement wavefield. The contribution of the P wave is shown in red and the S wave is in green. The wave components are superposed on a representation of the 2-D structural model. The individual snapshots give direct

GJI000 16/11/98 13:22:53 3B2 version 5.20
The Charlesworth Group, Huddersfield 01484 517077

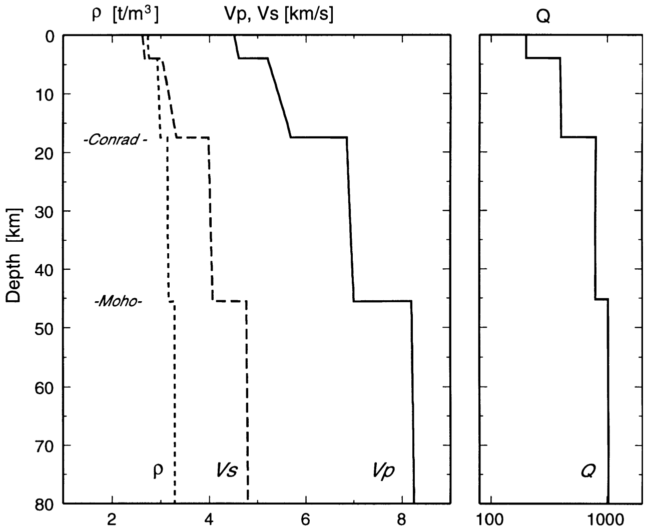

Figure 4. The depth variation of P-wave (V_P) and S-wave velocity (V_S), density (ρ) and the anelastic attenuation factor (Q) used in the 2-D numerical modelling for the shield reference structure.

insight into the characteristics of the wave propagation, including the role of conversions between P and SV waves produced at structural boundaries.

3.1 Seismic wave propagation in the shield model

Wavefield snapshots for the 2-D shield model are displayed in Fig. 5(a) with a regular time interval between frames, extending until the *Lg* phase approaches the edge of the frame.

In the upper frame (3 s) we see the radiation of P and S waves from the double-couple source in the crust, which give rise to large *Pg* and *Pn* phases propagating in the crust (24 s frame). By 45 s a large *Lg* phase complex has built up from multiple *SmS* reflections between the free surface and the Moho. The clear *Lg* disturbance can be tracked across the remaining frame sequence. The influence of the strong velocity jump in the Conrad discontinuity leads to the S-wave energy that forms the *Lg* phase being almost entirely trapped within the upper crust and this means that the group velocity of *Lg* is reduced to 2.5–3.2 km s^{-1} from its typical continental value of 3.5 km s^{-1}. The separation of the *Sn* head wave from the *Lg* wave complex is also seen. In later frames this faster S-wave arrival leads to strong *Sn*-to-P conversions in the surficial layer.

The *Pn* mantle and *Pg* crustal waves reach the basin of Mexico City by the 66 s frame, but are not much affected by the shallow heterogeneity. In comparison, the influence on S is much stronger. With the passage of the *Sn* phase (87 s) and the *Lg* wave (108 s) across the sedimentary basin, significant scattering associated with *S-to-P* conversion at the edge of the basin (e.g. at 129 s) is seen and the amplitude of the P and S waves in the basin is considerably enhanced. The *Lg* wave passing through the basin is somewhat weakened by the removal of S-wave energy by scattering into the basin and its leakage into the mantle (129 s). *Lg* has nearly recovered its amplitude in the last frame (150 s).

The fundamental Rayleigh *Rg* wave, propagating in the uppermost crust, behind the *Lg* wave is very weak for the source at 17 km depth. *Rg* can be seen most clearly in later snapshots (66–150 s), and is barely affected by passage through the small sedimentary basin.

3.2 Seismic wave propagation in a subduction zone

Snapshots of the P and SV wavefield for the 2-D model are shown in Fig. 5(b), including a subduction zone for the same times as in Fig. 5(a). The same plotting parameters are used as in Fig. 5(a), so that the changes in the wavefield produced by the presence of the subducting plate can readily be seen by comparison with the corresponding snapshots for the shield.

In the 24 s time frame there are much larger P and S waves radiating from the source in the subduction zone. This energy is efficiently guided into the crust along the dip of the subducting plate, which produces much larger crustal *Pg* and *Lg* phases than those seen in the shield model (24, 45 s). The amplitudes of the mantle phases *Pn* and *Sn* are rather small in the first few frames (24, 45, 66 s) for the subduction model. The large crustal heterogeneity at the left-hand side of the model hinders the transfer of energy into the mantle.

However, once the seismic phases have penetrated into the shield zone on the right-hand side of the model beyond 170 km from the epicentre, we can see the large *Pn* and *Sn* phases (see the 45 and 66 s frames). The *Lg* phase for the subduction model also has a very large amplitude compared to that in the shield model (see the 87 and 108 s frames); the wedge formed by the subduction zone has acted to enhance the energy radiating into the continental crust.

As an *Sn* wave enters the sedimentary basin it produces significant P conversions (87 s). In later frames we note the quite complicated wavefield in the near surface produced by scattering.

3.3 Synthetic seismograms and peak-amplitude attenuation

For the shield and the subduction models we compare the synthetic seismograms of the vertical and radial components of ground velocity motion at the surface as a function of epicentral distance in Fig. 6, together with the peak amplitude for each seismogram.

We also indicate the attenuation to be expected from the empirical relation proposed by Ordaz & Singh (1992). Since the geometrical attenuation for a 2-D model is slightly weaker than that for an actual 3-D wavefield, we employ the square root of the empirical value to obtain a rather gently sloping reference attenuation curve for the 2-D wavefield.

3.3.1 Shield model

In the synthetic seismograms of vertical and radial components for the shield reference model (Fig. 6a) the *Pn* head wave as a first arrival is clearly seen on the vertical and radial components with a group velocity of around 8.0 km s^{-1}. The *Sn* wave is also clear with a phase velocity around 4.5 km s^{-1}, and is followed by an *Lg* wave train formed by a number of *SmS* reflections between the free surface and the Moho, which have a broad group velocity range between 3.2 and 2.5 km s^{-1}. There is also a weak *Rg* phase with a slower group velocity below 2.5 km s^{-1}. The *Lg* wave entering the basin of Mexico City is somewhat enhanced in both amplitude

GJI000 16/11/98 13:22:54 3B2 version 5.20
The Charlesworth Group, Huddersfield 01484 517077

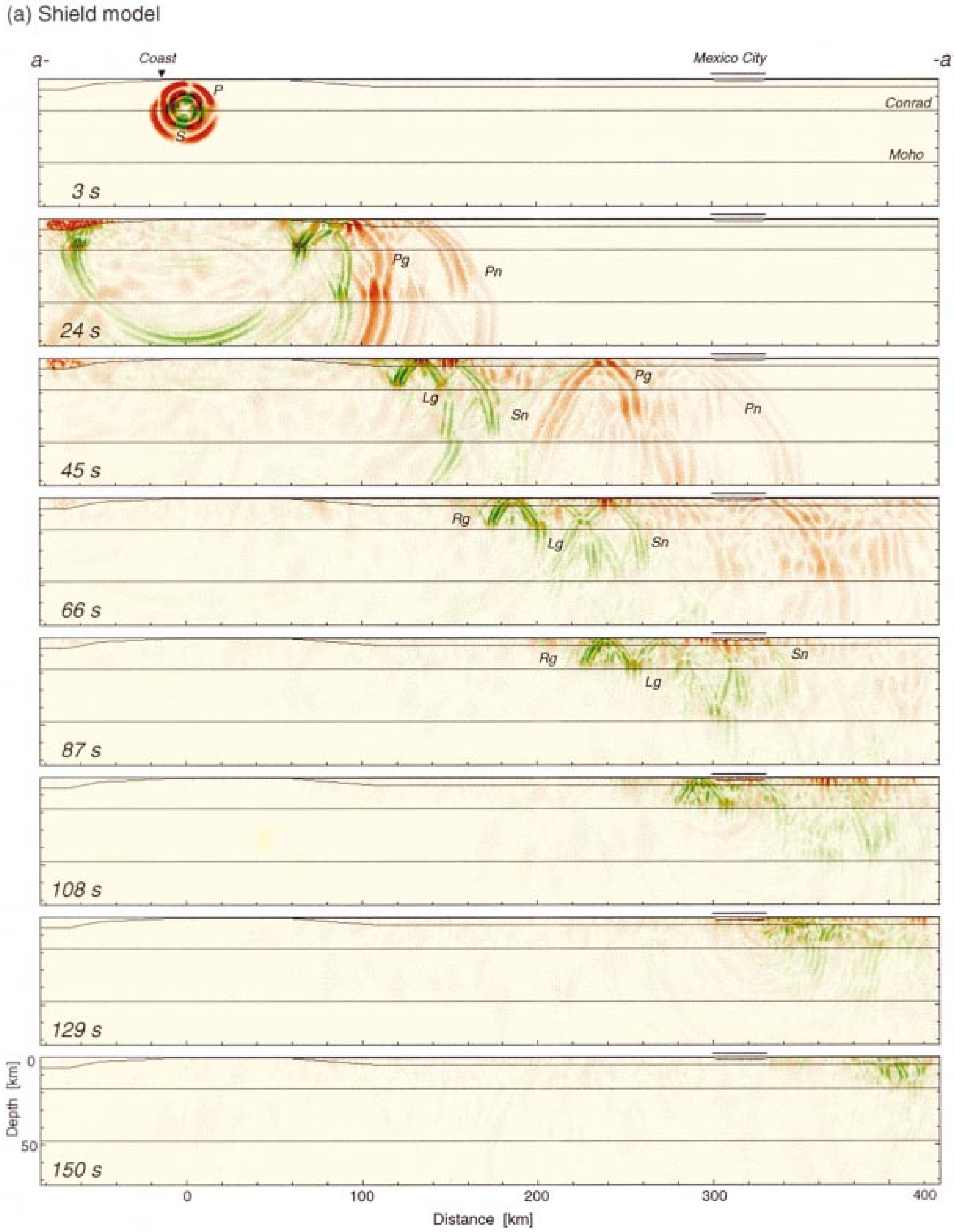

Figure 5. Snapshots of the seismic wavefield illustrating the *P* and *SV* components of the wavefield as a function of distance from source and time; the *P*-wave contribution is shown in red and the *S*-wave contribution in green. A double-couple source is placed 17 km below the free surface (a) for the shield model and (b) for the simple subduction model. The location of Mexico City between 300 and 320 km from the epicentre is marked in the figure.

and duration of the wave, but is rather weaker than the observations.

The peak amplitudes of both the vertical and the radial components are slightly weakened after passing through Mexico City, and gradually recover as the distance from the basin increases.

3.3.2 Subduction model

The change in the character of the regional wavefield as a result of the significant crustal heterogeneity introduced by the presence of the plate subduction is clearly seen in the synthetic seismograms displayed in Fig. 6(b) when compared with the waveform for the shield model (Fig. 6a). The changes in the seismograms are much stronger for the radial component. For instance, the *Sn* phase for the subduction model has a significant amplitude at a distance range of 230–320 km. The character of *Lg* waves in the subduction model is modified from the shield model since the multiple surface reflections of *S* on the left-hand side of the model are changed by the wedge of the crustal waveguide.

For the subduction model, there is a large *Sn*-wave arrival at a distance range of 230–400 km that increases in amplitude at larger distances. The peak amplitude for the radial component drops rapidly on emergence from Mexico City but recovers

GJI000 16/11/98 13:22:55 3B2 version 5.20
The Charlesworth Group, Huddersfield 01484 517077

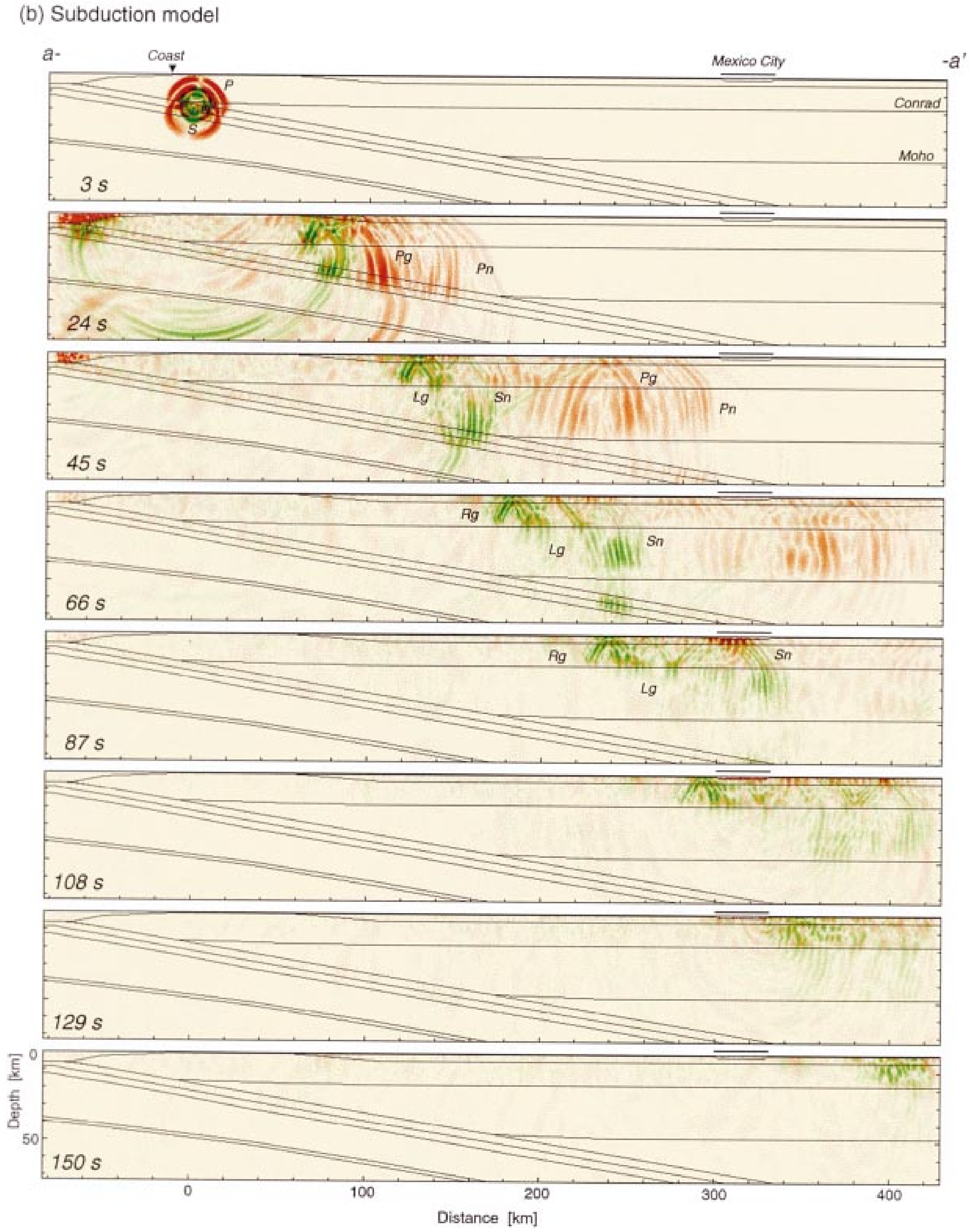

Figure 5. (*Continued.*)

its amplitude at greater epicentral distances. The pattern of peak velocity for the vertical and radial components for the subduction model is similar to the observations (Figs 2a and 3), which show an increase in amplitude for distances beyond 220 km and a sudden drop for stations just beyond Mexico City.

The lateral structural gradient induced by the presence of the dipping subducting plate leads to an enhancement of *P*- and *S*-wave energy in the lower crust compared to the simple shield model. Once the waves pass into the shield structure some 200 km away from the source, this energy is transferred to shallower levels in the crust, reinforcing the surface amplitude, so the peak amplitude at larger distances is enhanced compared with shorter distances.

In both the shield model and the subduction model, there is strong amplification of the *Sn* and *Lg* waves entering the basin of Mexico City with its low-velocity sediment. *Lg* coda is also extended for Mexico City stations and lasts for more than 40 s from the onset of the *Sn*-wave arrival to the end of the coda.

3.4 Effect of the subducting plate

In order to try to understand the mechanism that leads to efficient transport of seismic energy along the dip of the subducted plate, we have constructed two models that include only part of the structure of a realistic subducting plate. In the first case we include only an inclined high-velocity and low-attenuation oceanic lithosphere and in the second we include

GJI000 16/11/98 13:22:57 3B2 version 5.20
The Charlesworth Group, Huddersfield 01484 517077

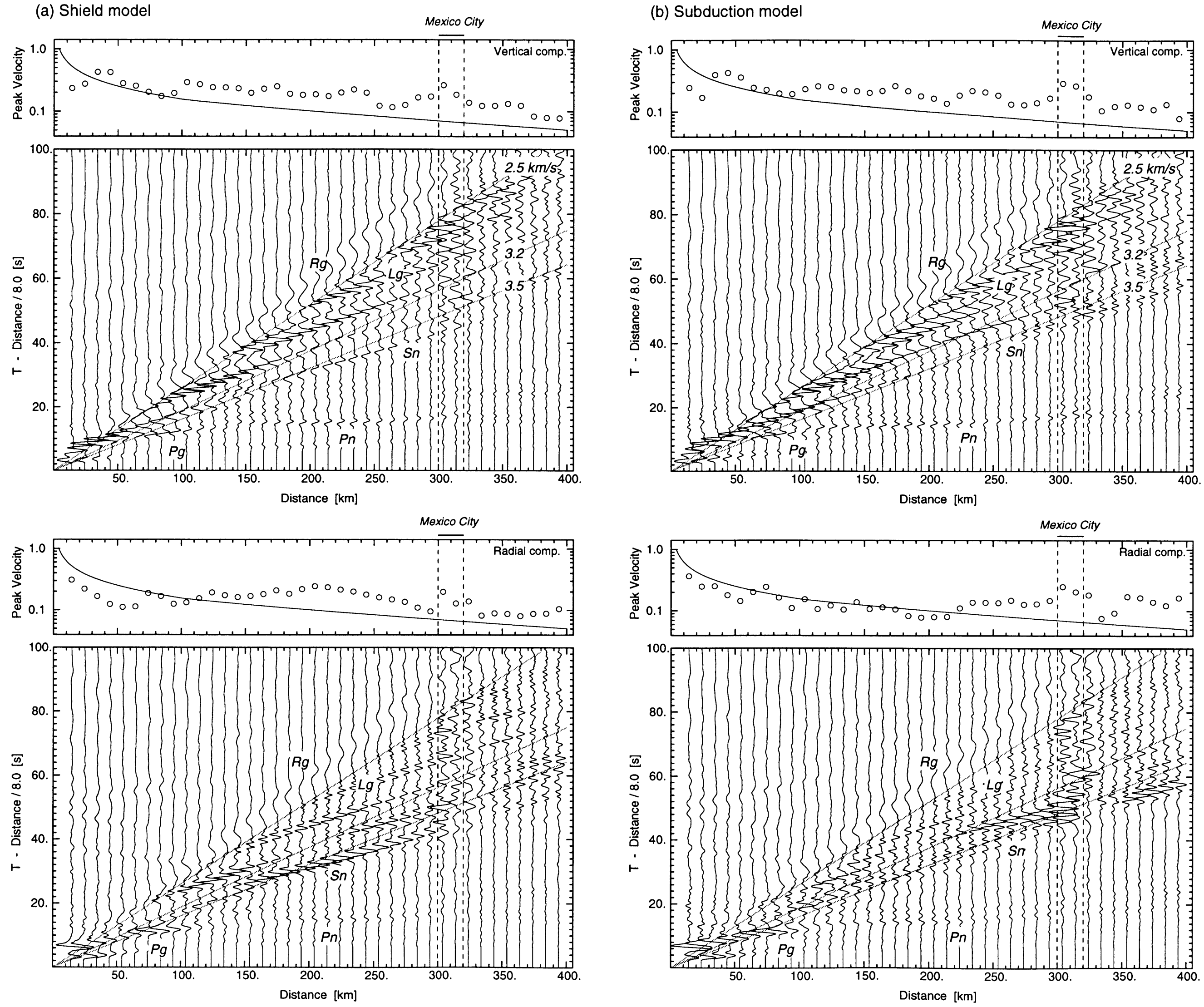

Figure 6. Synthetic velocity seismograms for vertical and radial components calculated by 2-D pseudospectral modelling (a) for the shield model and (b) for the simple subduction model. The major phases are marked. The location of Mexico City is shown. The peak amplitude of each trace is plotted as a function of distance from the epicentre. The empirical amplitude decay curve for 2 s period derived by Ordaz & Singh (1992) is superposed. Group velocities of 3.5, 3.2 and 2.5 km s^{-1} are indicated.

only the thin layer of the oceanic basalt and the oceanic upper crust, with low velocities and high attenuation.

We show a sequence of snapshots for the *P–SV* wavefields and synthetic seismograms for just the radial component because, as seen in the previous experiments, the wave shape for radial motion is more sensitive to the variation in crustal structure.

3.4.1 *Effect of a higher-velocity subducting plate*

When the plate has a simple structure with just high-velocity oceanic lithosphere, there is a sharp velocity contrast between the crust and the top of the plate, producing clear *S* reflections between the free surface and the subducting plate surface (Fig. 7a, the 'V' shapes in the upper crust in the 90 s frame). This process leads to an efficient ducting of *S*-wave energy along the dip of the subduction into the homogeneous crust to the right of the model.

In the radial-component seismograms, the regular pattern of multiple *S*-wave arrivals is seen, which produces coherent *Sn* and *Lg* wave trains (Fig. 7a). However, the character of the wavefield displayed in the snapshots and synthetic seismograms for this simple subduction model differ significantly from the previous results (Figs 5b and 6b), which included the full subduction structure.

3.4.2 *Effect of a low-velocity layer in the subducting plate*

The second model includes only the influence of the thin lower-velocity layer (LVL) that forms the upper part of the subducted plate (Fig. 7b). In the snapshots for this case the *S*-wave energy efficiently trapped within the LVL in the subducted plate (30, 60 s) is clearly seen.

As the *S* wave front reaches the intersection of the Moho with the subduction zone (about 180 km from the source), the *S* wave in the crust separates from the *S* wave in the LVL. The

GJI000 16/11/98 13:22:58 3B2 version 5.20
The Charlesworth Group, Huddersfield 01484 517077

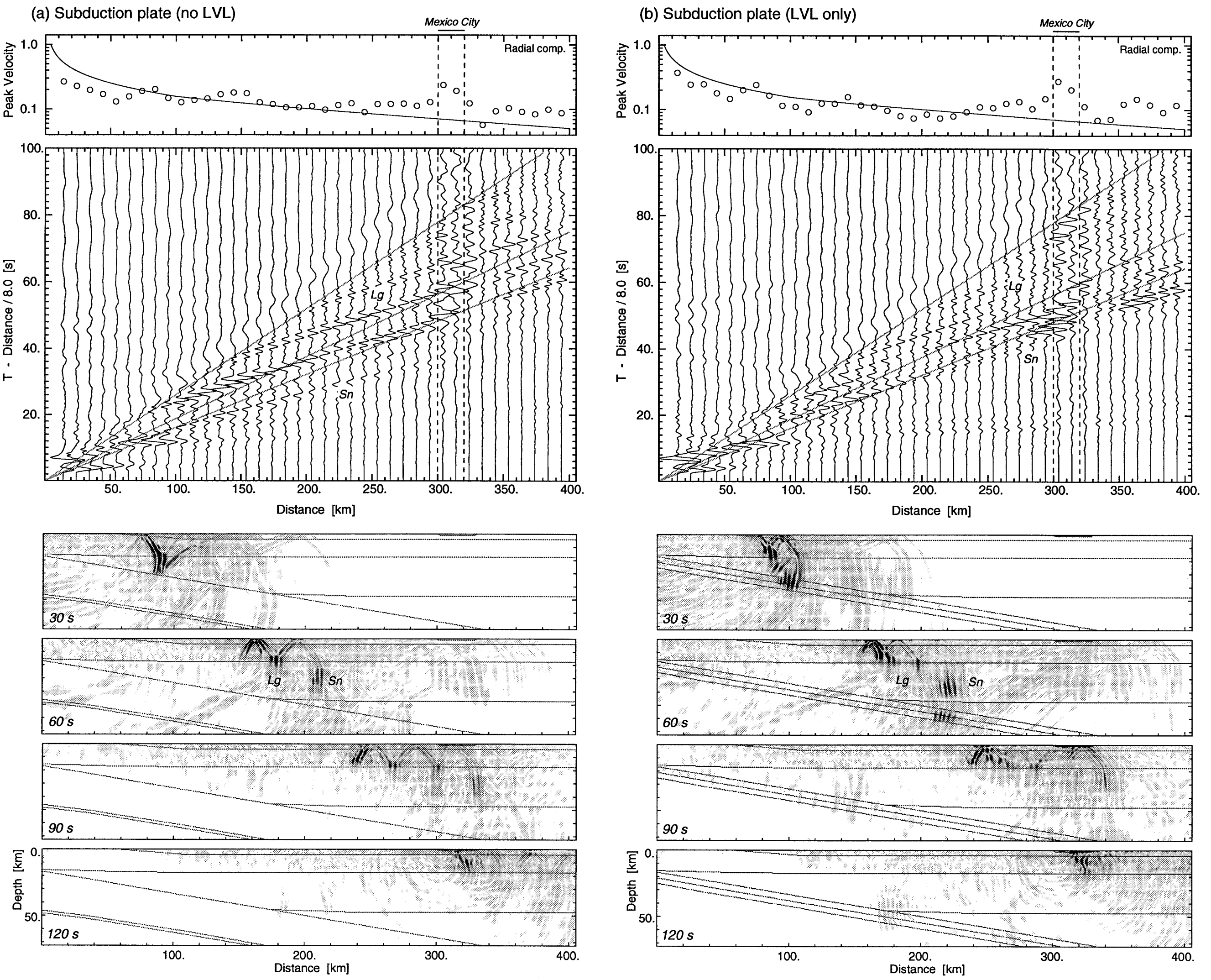

Figure 7. Synthetic velocity seismograms for the radial component, the peak amplitude and snapshots of the seismic wavefield for (a) the subducting plate excluding the upper low-velocity layer (LVL), and (b) subduction of a thin LVL.

result is that *S*-wave energy escaping from the LVL returns to the crust, producing a large *Sn* arrival at the surface (90 s). There is a strongly curved *Sn* wave front linking back to the LVL (60 s) due to the sudden change in the *S* wave speed between the LVL and the mantle. The refraction bends the *Sn* wave front toward the horizontal so that the amplitude of the *Sn* wave on the radial component is strongly increased (90 s frame).

Consequently, both of the components of the subducted plate, the high-velocity oceanic lithosphere and the thin upper LVL, play an important role in guiding seismic energy into the crustal waveguide and by modifying the effective radiation pattern from the source to produce a complicated pattern of wave propagation at regional distances.

4 SEISMIC WAVE PROPAGATION WITH VARIATIONS IN THE CRUSTAL STRUCTURE

We have also examined the influence of other classes of heterogeneity in order to understand their influence on the wavefield and so improve the simulation of the observations. First we consider the influence of surface topography with a low-velocity surficial layer and then we look at the influence of the Conrad discontinuity.

4.1 Effect of surface topography

We include surface topography along the profile with a maximum height of 2 km above sea level, and a surficial layer of thickness 2 km to represent the Mexican Volcanic Belt (MVB) with slow V_S (Shapiro *et al.* 1997) and small attenuation (Yamamoto *et al.* 1997). This surficial layer ($V_P = 3.8$ km s^{-1}, $V_S = 2.2$ km s^{-1} and increased attenuation $Q = 300$) starts at 240 km beyond the epicentre (60 km from Mexico City) (Fig. 8a).

In the 90 s snapshot frame in Fig. 8(a) the *Sn* and *Lg* waves are seen entering the surficial layer. This produces significant *P* and *S* scattering within the zone, which leaves a clear trail in the synthetic seismograms through large high-frequency seismic disturbances at later times. The *Sn* wave entering the low-velocity surficial layer is slightly weakened, while the effect of *Lg* is dramatically enhanced due to *S*-to-*P* conversions. The

GJI000 16/11/98 13:22:59 3B2 version 5.20
The Charlesworth Group, Huddersfield 01484 517077

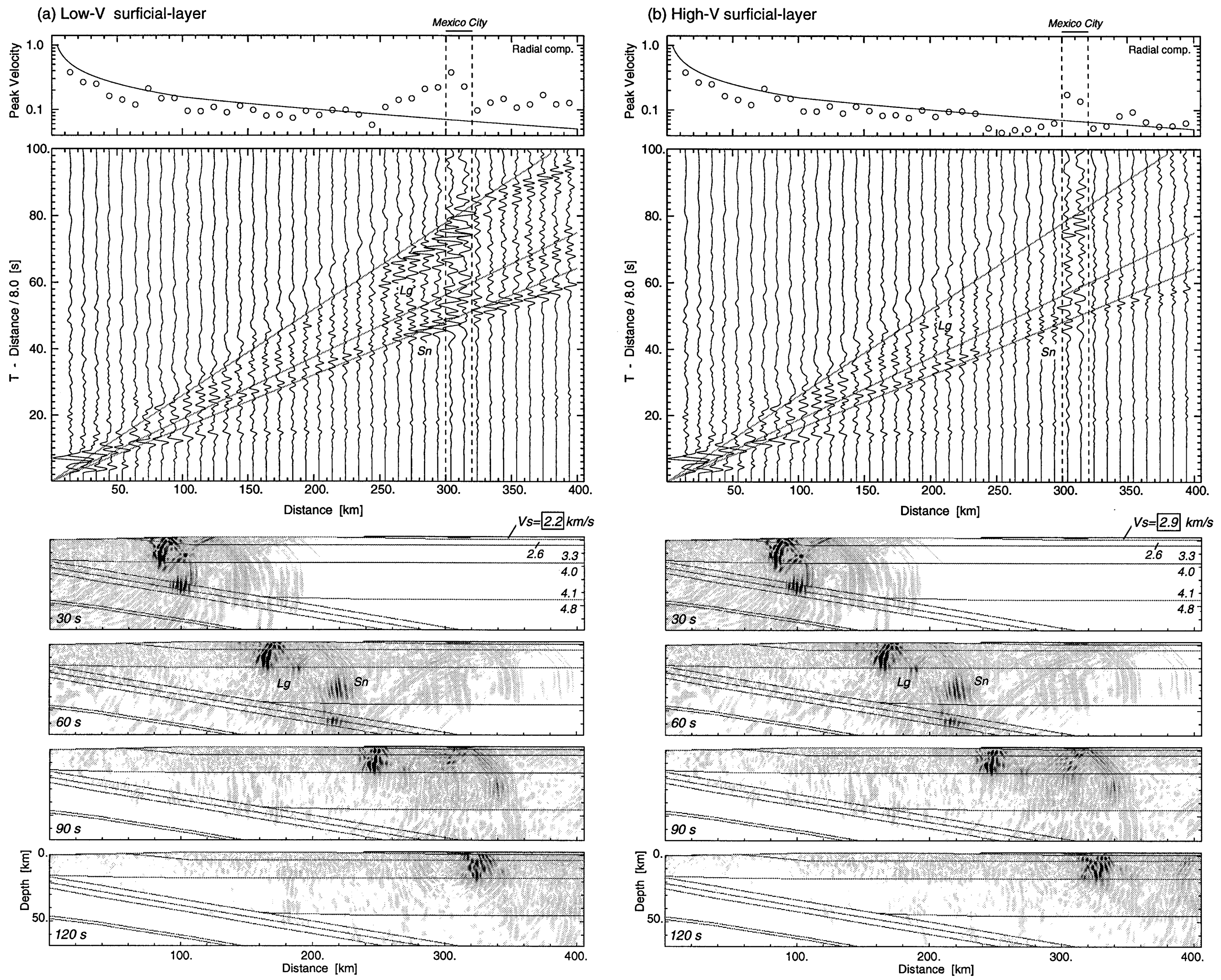

Figure 8. Synthetic velocity seismograms for the radial component, the peak amplitude and snapshots of the seismic wavefield for the model including a topography and surficial layer. (a) Lower-velocity ($V_S=2.2$ km s^{-1}) surficial layer; (b) higher-velocity ($V_S=2.9$ km s^{-1}) surficial layer. The *S*-wave velocity for each layer of the crust is indicated.

result is a longer and larger *Lg* wave train impinging on the basin of Mexico City, which produces significant ground shaking (120 s frame). Such an influence of topography and near-surface geology on the enhancement of *Lg*-wave coda has been noted in a number of other studies (e.g. Olsen *et al.* 1983; Campillo 1987; Zang & Lay 1994; Goldstein *et al.* 1997).

The amplification of the *Lg* wave by lowered velocities in the surficial layer is confirmed by comparison with an alternative model. In Fig. 8(b) we include higher-velocity material with $V_P=5.0$ km s^{-1}, $V_S=2.9$ km s^{-1} and $Q=300$ in the surface layer. The seismograms for this model show a considerable weakening of the *Sn* and *Lg* waves, even though their group velocities are almost unchanged.

Although there is a large change in the seismograms between Figs 8(a) and (b), the character of the *Lg* and *Sn* phases seen in the wavefield snapshots are almost unchanged. This indicates that the propagation of the *Lg* and *Sn* phases is controlled by the averaged structure of the crust, while the amplitude at the surface is very sensitive to the properties in the near-surface zone.

4.2 Effect of velocity structure in the lower crust

The base velocity model we have employed so far has been based on Valdes *et al.* (1986) and has a large velocity jump at the Conrad discontinuity at 17 km depth, where the *S*-wave velocity changes from 3.3 to 4.0 km s^{-1}; this is accompanied by a rather small velocity gradient in the lower mantle (Fig. 4). The consequence is that the *Lg* wave has its energy concentrated within the upper crust as can clearly be seen in the snapshots in Figs 5(a), (b), 7 and 8. This behaviour is rather different from that seen in more typical continental crustal models (see e.g. Furumura & Kennett 1997, Fig. 2a). We also evaluated the sensitivity of the regional *Sn* and *Lg* phases observed on the surface to changes in the velocity structure deep in the crust.

We have therefore modified the velocity structure around the Conrad discontinuity, assigning it a smaller velocity jump, from 3.3 to 3.6 km s^{-1}, and consequently a larger velocity gradient in the lower crust (Fig. 9a). The effect of the enhanced velocity gradient in the lower crust is to modify the character of

GJI000 16/11/98 13:23:00 3B2 version 5.20
The Charlesworth Group, Huddersfield 01484 517077

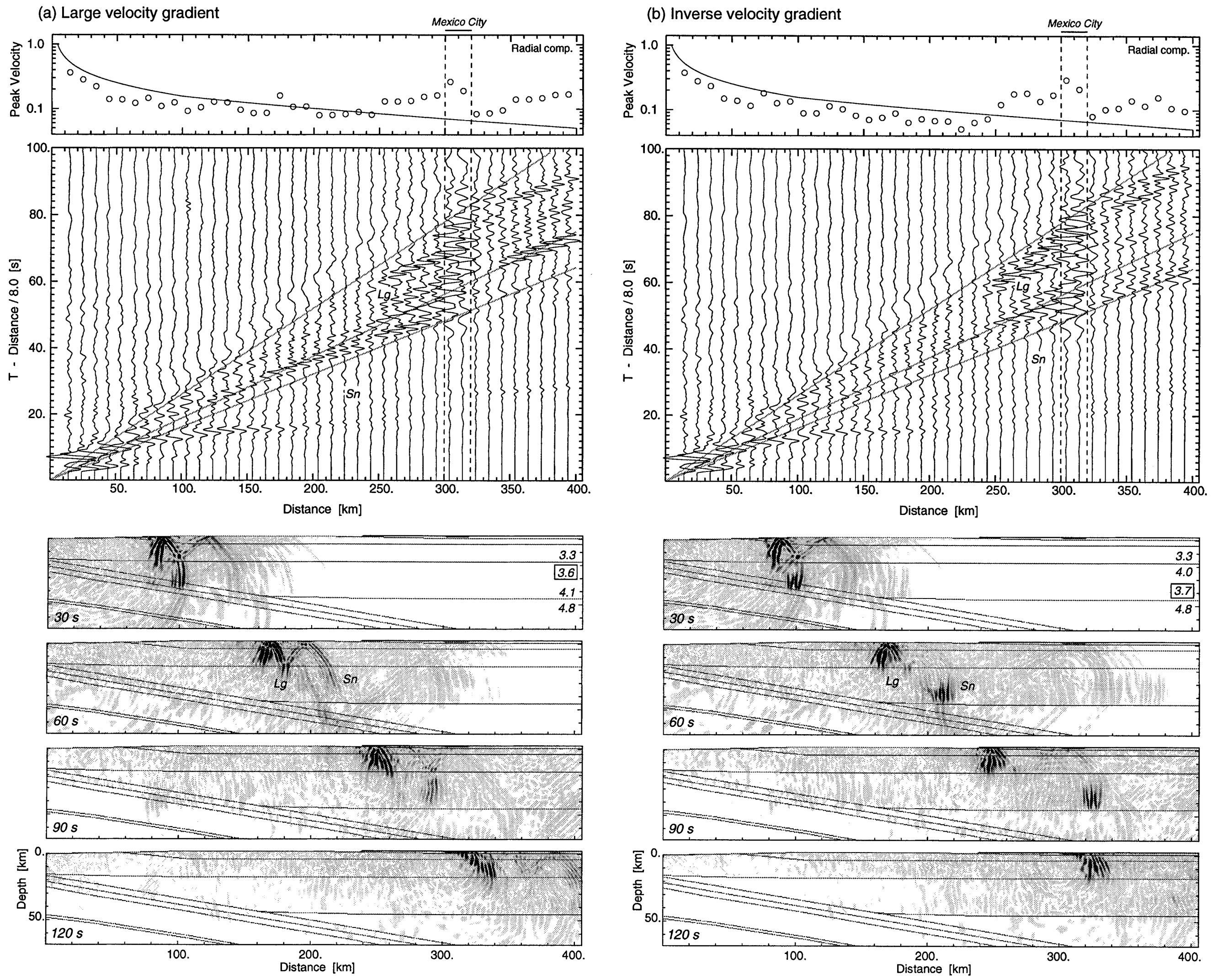

Figure 9. Synthetic velocity seismograms for the radial component, the peak amplitude and snapshots of the seismic wavefield for models with different crustal velocities: (a) small velocity jump in the Conrad (3.3–3.6 km s^{-1}) with a large velocity gradient in the lower crust (3.6–4.1 km s^{-1}); (b) negative velocity gradient in the lower crust (4.0–3.7 km s^{-1}). The *S*-wave velocity for each layer of the crust is indicated.

the *S* waves propagating in the crust so the energy extends widely through the crustal waveguide (compare the 60 s frame with Fig. 8a). The refraction of the *Sn* wave separated from the LVL in the subducted plate generates a very large *Sn* arrival at epicentral distances between 160 and 300 km. The peak amplitude of the *Lg* wave train for this model shows a much earlier arrival than for Fig. 8(a), with a group velocity of about 3.0 km s^{-1}, which is quite similar to the observations (Fig. 2a). The pattern of peak velocity with distance also has the general character of the observations, with an increase beyond 250 km from the epicentre and a sudden drop after passing through Mexico City (Fig. 3).

We have also examined the sensitivity of the *Sn* and *Lg* phases to the velocity structure in the lower mantle by employing a rather unusual model with a negative velocity gradient for *S* from 4.0 to 3.7 km s^{-1} in the lower crust (Fig. 9b). In the 60 and 90 s snapshots, there is a concentration of seismic energy within the low-velocity zone above the Moho, and as a consequence the *Sn*-wave amplitude observed at the surface is very small compared to the previous models. The lower crust with a negative velocity gradient over the strong velocity jump over the Moho acts as a perfect waveguide for the *Sn* waves. The *Lg* waves are not unduly affected by the lower-crustal velocity anomaly, and are close in form in both snapshots and synthetic seismograms to Fig. 8(a).

5 INFLUENCE OF CRUSTAL HETEROGENEITY WITH VARYING SOURCE DEPTH

The previous simulations have employed a fixed source representation with a single source mechanism and depth. However, the nature of the source plays an important role in the interaction of the seismic wavefield with the lateral heterogeneity in the crustal waveguide. We have therefore performed a set of numerical experiments with the crustal models from the previous sections, but with various source types and depths in the crust.

GJI000 16/11/98 13:23:01 3B2 version 5.20
The Charlesworth Group, Huddersfield 01484 517077

We use the seismic reciprocal theorem to construct a set of waveforms for a single receiver position placed at the centre of Mexico City corresponding to many different source depths in a single calculation (Furumura & Takenaka 1990). We display seismograms for sources at a fixed horizontal range of 300 km from the centre of Mexico City with a range of source depths between 0 and 46 km.

5.1 Shield zone

The first model we consider is a shield zone produced by extending the shield structure on the right of Fig. 9(a) across the full width of the model to provide a reference for comparison with the presence of a subduction zone. We consider sources on a shallow-angle thrust fault, as in the 1985 Michoacan and 1995 Copala events.

The set of reciprocal seismograms, for both vertical and radial components (Fig. 10a), shows the way in which the relative arrivals of the regional phases are influenced by the source depth for a fixed source mechanism. The first arrival is a small mantle *Pn* phase followed by a crustal *Pg* phase; these *P* phases have almost the same amplitude for all source depths in the crust.

The mantle *Sn* phase has a very large amplitude on the radial component when the source is located close to the surface. The *Lg* phase is a prominent feature for both vertical and radial components for the source excited in the upper crust, with a generally larger vertical component. However, when the source lies in the lower crust the radial component of *Lg* is more prominent. A relatively long *S* wave train is built up from *Sn* and *Lg*-wave coda for all source depths in the upper crust. The duration and amplitude of the *S* wave train is gradually weakened when the source is located in the lower crust.

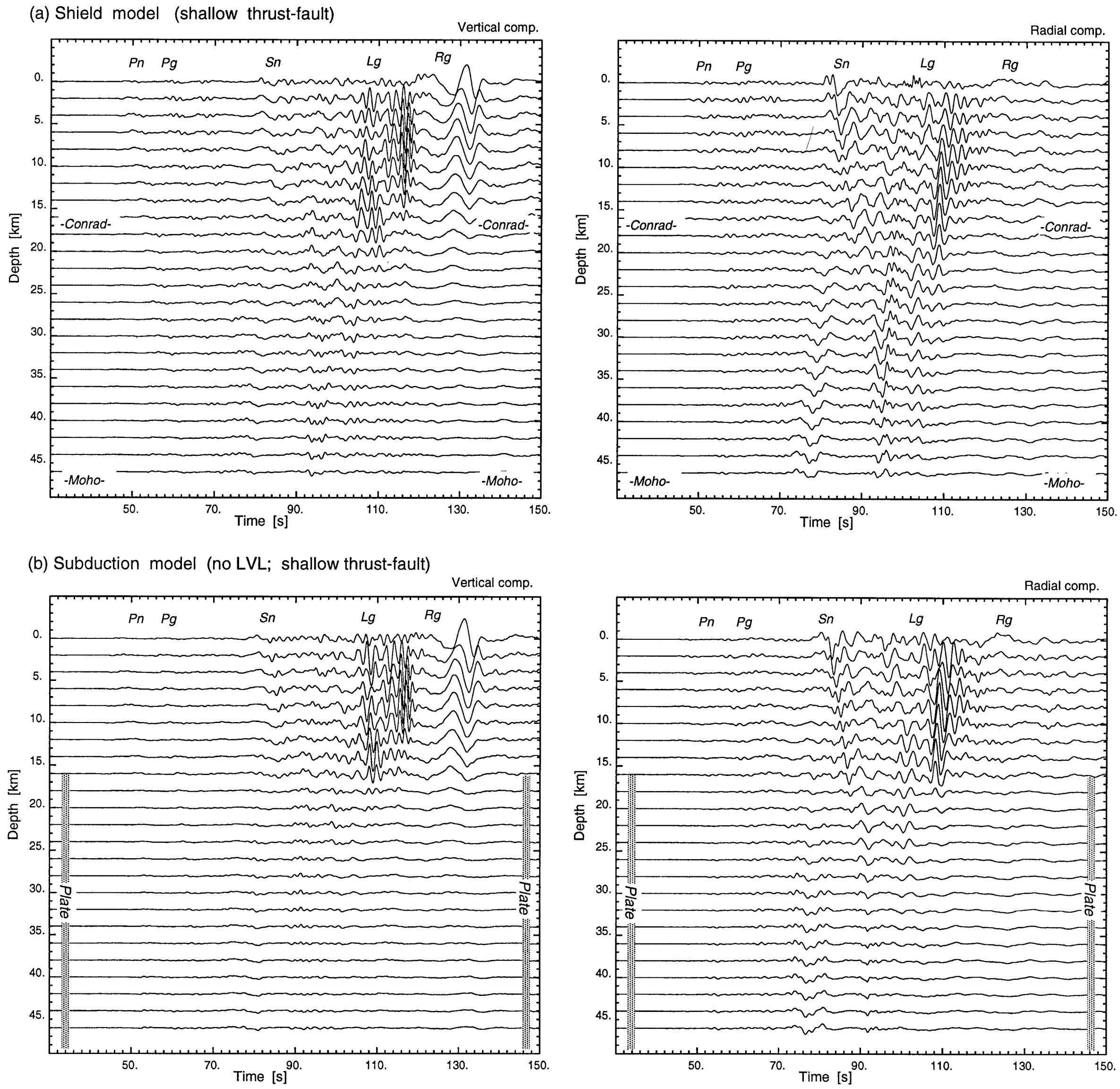

Figure 10. Synthetic velocity seismograms of vertical and radial components for a distance of 300 km from a double-couple source illustrating the change in the characteristics of each regional phase with source depth for (a) a shallower-angle thrust-fault source in the shield model, (b) the subduction model excluding the upper LVL, (c) the same as (a) but for the full subduction model, and (d) a normal-fault source. The locations of the Conrad discontinuity, the Moho and the subducted plate are marked.

GJI000 16/11/98 13:23:02 3B2 version 5.20
The Charlesworth Group, Huddersfield 01484 517077

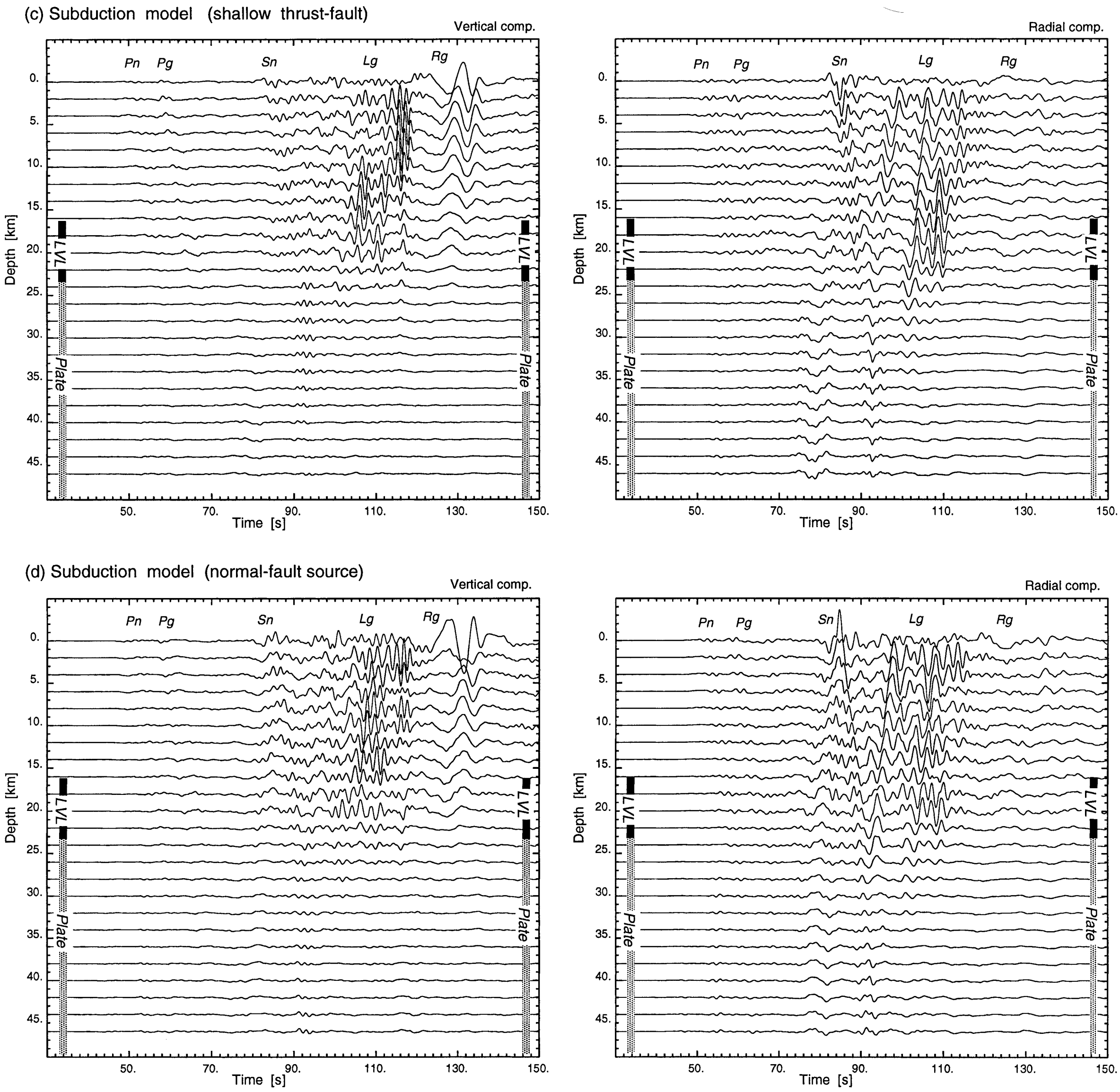

Figure 10. (*Continued.*)

The fundamental Rayleigh wave *Rg* has a very large amplitude on the vertical component that decreases rapidly as the source depth increases.

5.2 Subduction zone

With the presence of a subducting plate there is a very significant change in the character of the regional phases as a function of source depth. Now the *S*-wave energy radiated from the source excited over the plate can be guided into the crust by multiple reflections along the dip of the plate. We start by considering shallow thrust sources.

In the reciprocal seismograms (Fig. 10b) for a subduction model without a low-velocity upper layer, the *Sn* and *Lg* phases on the radial component for sources located in the upper crust are enhanced compared to Fig. 10(a). The amplitudes of the *S*-wave coda on both the radial and the vertical components are suddenly weakened when the source is located in the plate. The *Rg* wave is barely affected by the heterogeneity in the lower crust since the fundamental surface wave is almost entirely confined to the upper crust.

When the low velocity zone is reinstated (Fig. 10c) in the subducting plate there is an enhanced *S* wave train when the source lies in the depth range of the LVL. For this depth interval there is larger excitation of the *Lg* waves on the radial component than for shallower sources. As a final example, we consider a sequence of normal-fault sources in the full subducted plate model (Fig. 10d). The seismograms show a similar pattern of wave amplitude with source depth as Fig. 10(c), even though the radiation patterns of *P* and *S* from the source are completely different from the previous thrust-fault source. The wave shape and the time of the amplitude maximum differ slightly from the previous model (Fig. 10c).

These results indicate that the large, long-duration ground shaking in Mexico City for the laterally heterogeneous waveguide, as shown in the previous sections for the 17 km deep thrust fault, will be sustained for all source depths and

GJI000 16/11/98 13:23:02 3B2 version 5.20
The Charlesworth Group, Huddersfield 01484 517077

mechanisms in the upper crust. Moreover, the *Lg*-wave amplitude for radial ground motion is considerably enhanced when the source lies in the LVL in the subducting plate.

6 3-D SIMULATION OF THE MEXICAN EARTHQUAKES

In order to examine the way in which 3-D structure may influence the complex propagation character of the regional phases, we have modelled the seismic wavefield using a 3-D pseudospectral code (Furumura *et al.* 1996, 1998) to simulate the effects of the 1995 Copala and 1985 Michoacan events.

The 3-D model is 537.6 km wide by 537.6 km long by 102.4 km deep and has been discretized with uniform grid intervals of 2.1 km in the horizontal coordinates and 1.6 km intervals in the vertical direction. The main model is surrounded by a suitable absorbing buffer zone following Cerjan *et al.* (1985) to eliminate artificial reflections from the boundaries.

The crustal structure for the 3-D model is developed from the previous 2-D structural model (Fig. 9a) including spatial variation in the depth of the Cocos Plate from Pardo & Suárez (1995). This model includes spatial variation of a 4.8 km thick and about 80–200 km wide surficial layer which models the Mexican Volcanic Belt with relatively slow velocities ($V_P=4.3$ km s^{-1}, $V_S=2.5$ km s^{-1}) and an anelastic attenuation factor of $Q=300$ (Yamamoto *et al.* 1997).

In order to simulate 3-D wave propagation on a large scale, we made some modifications to the model:

(1) we exclude the surface topography since we have adopted a rather large grid spacing;

(2) the water column in the offshore region is excluded from the model in order to increase the stability in the calculation of the large-scale model; we assigned rather fast wave velocities ($V_P=3.0$ km s^{-1}, $V_S=1.7$ km s^{-1}) and an anelastic attenuation factor of $Q=300$ in this region; and

(3) we use a simplified basin structure for Mexico City with a disc-like inclusion 31.5 km wide and 3.2 km deep with velocities $V_P=3.2$ km s^{-1}, $V_S=1.6$ km s^{-1} and an anelastic attenuation factor $Q=100$.

As a consequence we may underestimate the ground shaking in the basin of Mexico City and at the same time somewhat overestimate the ground motion in the offshore area, but these effects should be too small to affect the main features of wave propagation in Mexico itself.

6.1 3-D simulation of the 1995 Copala, Guerrero, Mexico earthquake

We first look at the evolution of regional wave propagation from the 1995 Copala earthquake ($M_W=7.4$), which has formed the basis of our 2-D simulations.

A shallow ($H=16$ km) point source with a double-couple mechanism was placed at the epicentre of the 1995 Copala event, which was located about 300 km from the centre of Mexico City (Fig. 1). The seismic source imparts seismic *P* and *S* waves for the $M_W=7.4$ earthquake ($M_0=1.1\times10^{27}$ dyne cm) with a maximum period around 3 s. The number of gridpoints per shortest wavelength for this model is 3, which is again sufficient for the pseudospectral simulation.

Snapshots of the surface ground motion extracted from the 3-D seismic wavefield are displayed in Fig. 11. They are separated as before into *P*- (red) and *S*- (green) wave contributions by using the divergence and curl of the wavefield. The same amplification factor has been used for plotting in each frame.

In the first frame (40 s) *Pn* and *Pg* propagate across the Mexican mainland and *Sn* and *Lg* propagate about 100 km beyond the epicentre. The propagation speeds of the phases penetrating the Mexican Volcanic Belt (MVB) tend to reduce and their wave amplitudes are somewhat enhanced in the low-velocity sediments (55 and 85 s frames).

The sequence of multiple reflections within the crust that builds up the *Lg* is strongly influenced by the presence of the MVB, and the duration of the *Lg* wave train is significantly prolonged by *S*-wave scattering and *Lg*-to-*P* conversions. The successive multiple *S* reflections contributing to *Lg* enhance the ground motion at the surface at discrete distances, as can been seen in the snapshots for 70, 100 and 130 s.

In the snapshots for 100 and 115 s, the *Sn* and *Lg* phases reach the basin of Mexico City and are strongly amplified in the low-velocity sediment. There are also strong *Lg* conversions to *P* and *S* in the basin, which extract *S*-wave energy from the *Lg*-wave packet. In the last frame (145 s) the *Lg* wave that has travelled right through the MVB has been weakened, and its wave shape broken up by scattering in the low-velocity zone. The *S*-wave energy removed from the *Lg* wave train is still reverberating within the basin.

The synthetic seismograms for surface ground velocity derived from the 3-D modelling are displayed in Fig. 12. Two profiles are presented, an inland line a–a′ from the epicentre to Mexico City (inland stations, Fig. 12a) and a coastal line b–b′ (coastal stations, Fig. 12b). In the seismograms for the inland stations (Fig. 12a) there is a prominent *Lg* wave on the vertical and radial components. Even though we recognize the limitations of the modelling of the low-velocity sediment in the basin of Mexico City, there is quite a large amplification of the *Lg* phase at the basin stations, and the duration of the *Lg* wave train in the basin is prolonged.

Along the coastal line the *Lg* amplitude is too small to be discerned in the seismograms (Fig. 12b). As discussed previously, the crustal thickness is rather thin for effective *S*-wave trapping and the *S* energy tends to leak into the subducted plate. In addition, we recall that the radiation of seismic *S* waves in the direction of the coastal line is rather weak.

The *Lg*-wave amplitudes from this 3-D model are much larger on the vertical components than on the horizontal components, which is somewhat different from the observations (Fig. 2). This may arise because we have used a rather longer-period source of 3 s and faster surficial layers due to the limitations of 3-D modelling.

Fig. 13 shows the distribution of the peak velocity at the surface for the vertical and horizontal components (vector mean of two horizontal motions) for the time span extending for 200 s from the source initiation. In this figure multiple zones of higher amplitude are clearly seen, mainly produced by the successive surface reflection of *S* waves contributing to the *Lg* wave train. The peak amplitude of ground motion is also somewhat enhanced in the MVB, and a further amplification occurs in the basin of Mexico City, surrounded by the MVB, to strongly enhance the ground shaking for both vertical and horizontal motion. Such an amplification

GJI000 16/11/98 13:23:03 3B2 version 5.20
The Charlesworth Group, Huddersfield 01484 517077

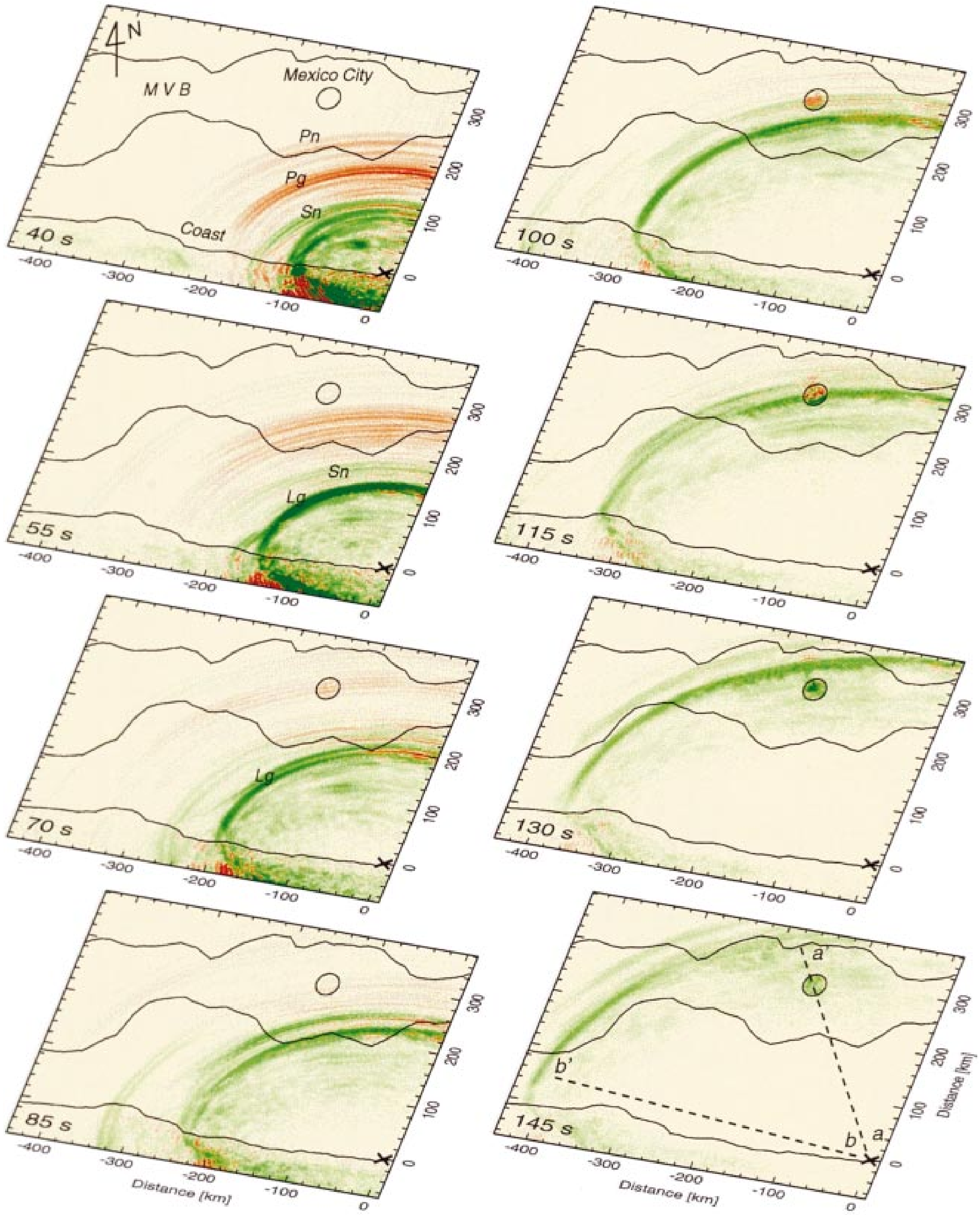

Figure 11. Snapshots of seismic wave propagation for the 1995 Copala, Guerrero earthquake calculated by the 3-D pseudospectral modelling illustrating the *P* and *S* waves at the surface. The *P*-wave contribution is shown in red and the *S*-wave contribution in green. The epicentre is marked in the bottom right corner by a cross. Distance is measured from the epicentre. The time from the source initiation is shown in the bottom left corner.

of peak ground motion in the MVB is also reported by Suter *et al.* (1996) from an analysis of a number of Mexican earthquakes.

The pattern of anomalous ground amplification with discrete highlighted zones is similar to that seen in California in the epicentral distance range below 100 km during the 1985 Loma Prieta earthquake, generated by critically reflecting *S* phases within the crust (Somerville & Yoshimura 1990), and is considered as the main cause of strong ground shaking in the San Francisco Bay region some 100 km away from the epicentre (Catchings & Kohler 1996). Our simulation results suggest that such distinct zones of high ground motion can also be produced by the components of the *Lg* phase at distances of 100–400 km from the epicentre.

We have also considered two variants on the configuration of the 1995 Copala event to see how the pattern of peak ground velocity is modified by using a somewhat deeper source or a source with a longer dominant period.

6.1.1 Deeper source

We consider a source at 25.6 km depth with a normal-fault source mechanism excited in the middle of the subducting plate and again calculate the 3-D wavefield. From the reciprocal

GJI000 16/11/98 13:23:05 3B2 version 5.20
The Charlesworth Group, Huddersfield 01484 517077

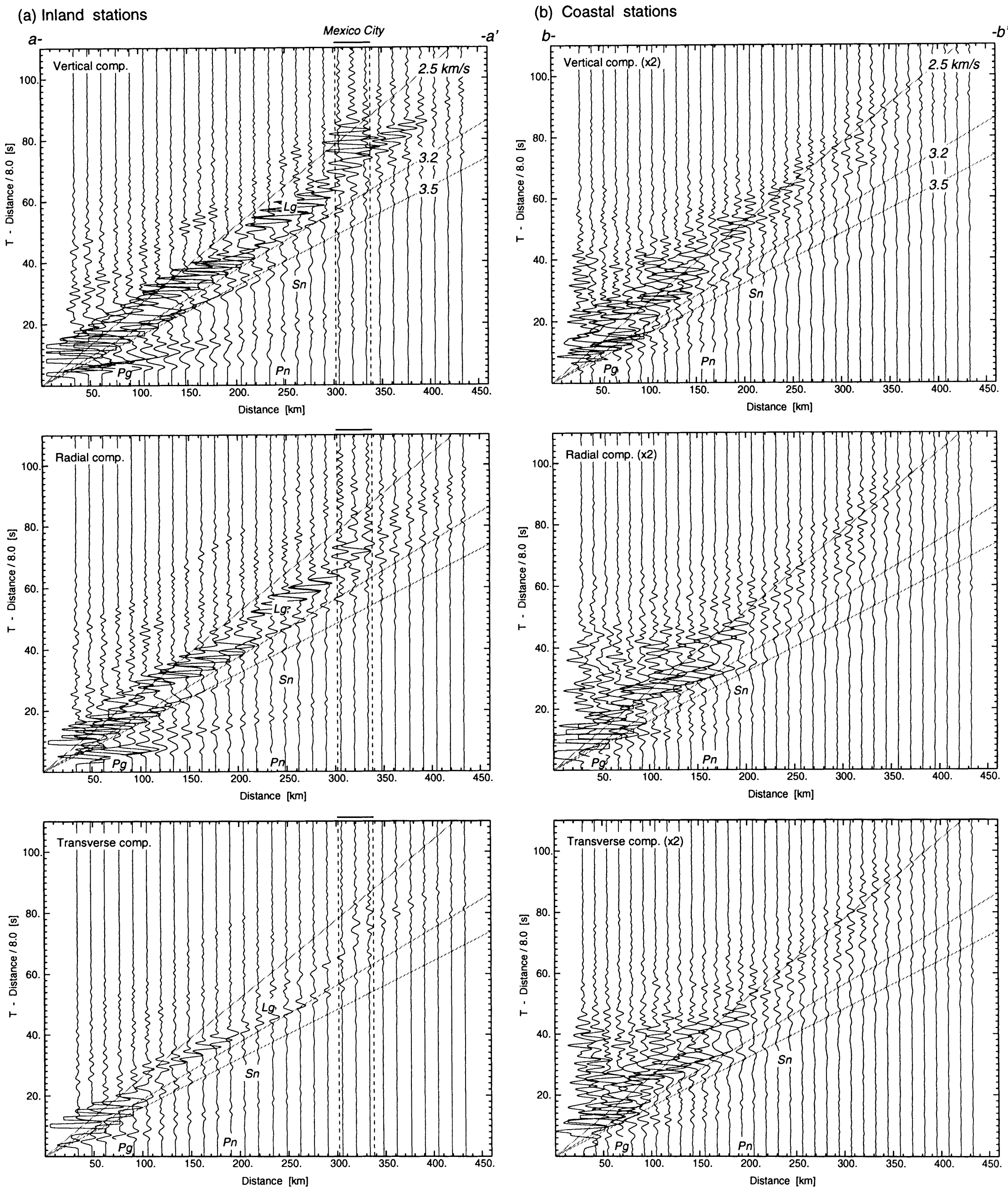

Figure 12. Synthetic velocity seismograms for vertical, radial and transverse components for (a) inland stations (a–a′ in Fig. 11) and (b) coastal stations (b–b′ in Fig. 11) (note that wave amplitude is multiplied by a factor of two.) Large phases are clipped. Group velocities of 3.5, 3.2 and 2.5 km s^{-1} are indicated.

seismogram calculations we expect that the results will be similar for a broad range of source depths within the plate. Events at depth within the subducting plate have often occurred in the Mexican subduction zone, such as the 1931 Oaxaca earthquake ($H=40$ km, $M_S=8.0$; Singh *et al.* 1985), the great Mexican earthquake of 1958 June 19 ($H=50$ km; $M\sim7.7$; Singh *et al.* 1996), and the 1994 Zihuatanejo earthquake ($H=50$ km, $M=6.6$; Cocco *et al.* 1997).

Fig. 14(a) displays the peak ground velocity motion derived from this deeper earthquake. The *Lg*-amplitude excitation from the deeper event is very weak and the dominant arrival in the regional wavefield is *Sn*, as already seen in the 2-D simulation (Fig. 10d). The pattern of peak amplitude has only one broad zone of high amplitudes modulated by the four-lobed *S*-wave radiation pattern from the double-couple source.

6.1.2 *Longer-period source*

We also examine the influence of the dominant frequency of the source, by considering the same source depth ($H=16$ km) and mechanism as in the main simulation (Figs 11–13) but with a dominant frequency of 0.1 Hz. This period lies on the edge of

GJI000 16/11/98 13:23:06 3B2 version 5.20
The Charlesworth Group, Huddersfield 01484 517077

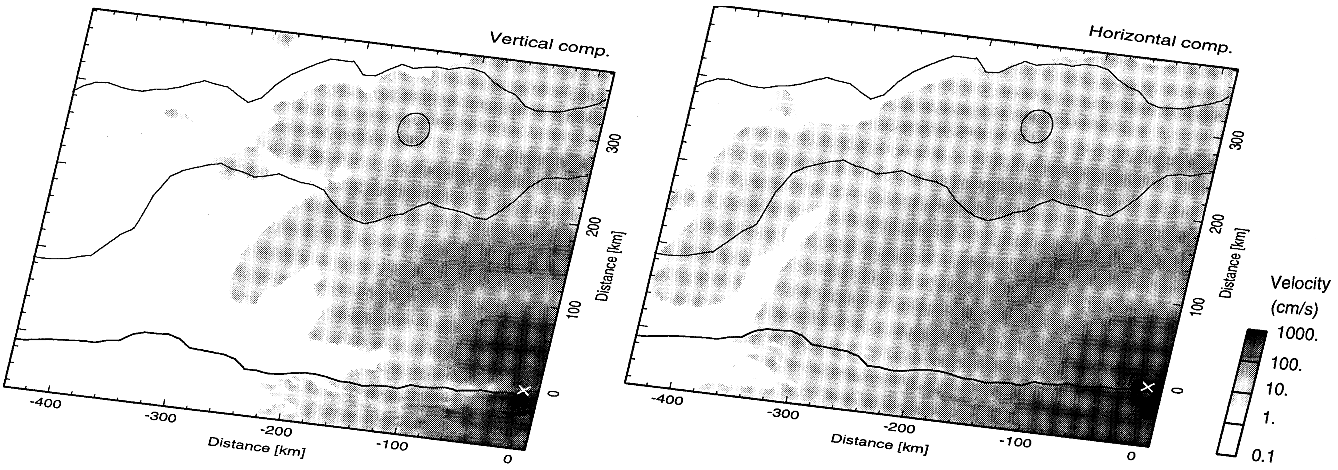

Figure 13. Maximum ground velocity distribution for the vertical (left) and the horizontal component (right) (vector mean of two components) of the 1995 Copala, Guerrero earthquake.

the normal frequency band for *Lg* from 0.1 to 5 Hz, and the power of the *Lg* wave is very small. In consequence, the peak-amplitude distribution (Fig. 14b) shows only a broad zone of high velocity around the source, similar to that from the deeper source (Fig. 14a).

From these simulations we can confirm that we need the combination of a shallower source ($H < 20$ km) and short-period waves ($T \sim 3$ s) to produce large amplitudes and long durations of *S* waves at distances around 300 km, and also the pattern of a set of discrete zones of high amplitude.

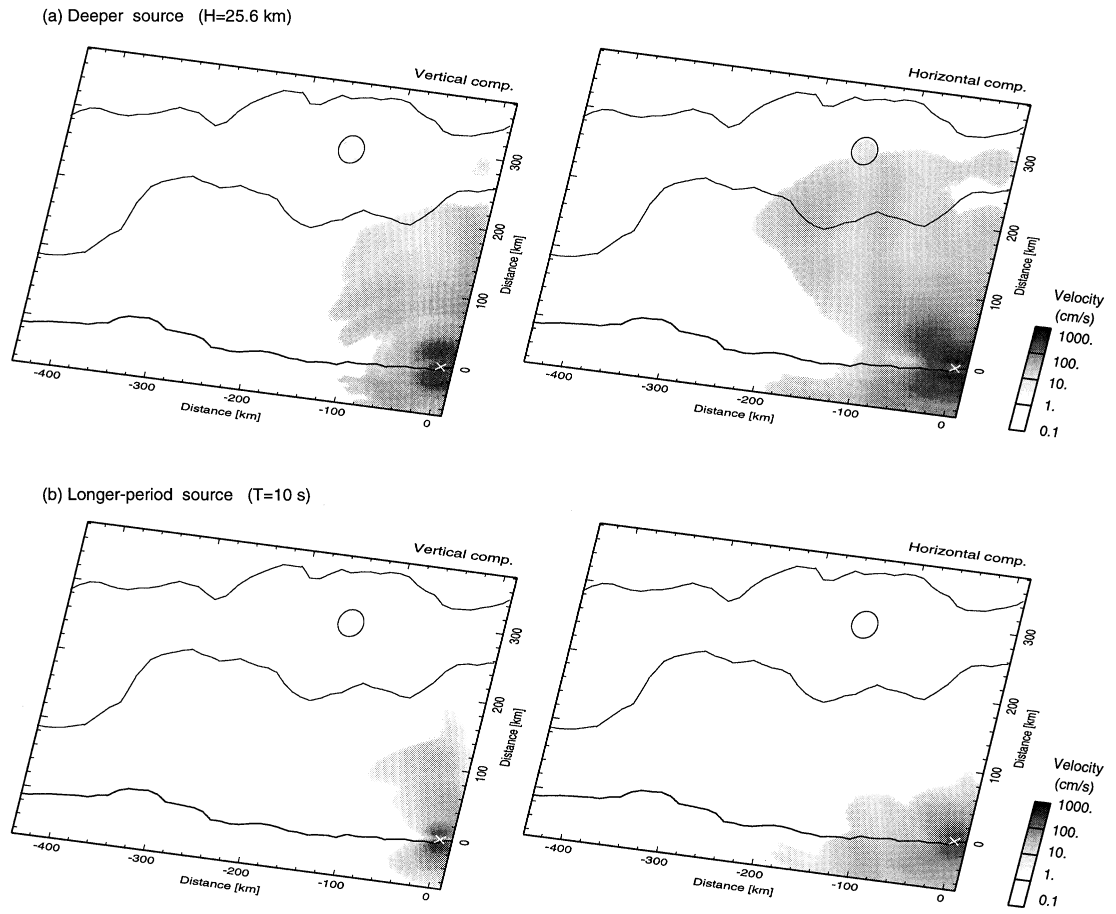

Figure 14. Maximum ground velocity distribution for vertical and horizontal components derived from (a) a source at 25.6 km depth and (b) the source radiating a longer-period wave ($T = 10$ s).

GJI000 16/11/98 13:23:07 3B2 version 5.20
The Charlesworth Group, Huddersfield 01484 517077

6.2 3-D simulation of the 1985 Michoacan earthquake

The second 3-D computation represents a simulation of the great 1985 Michoacan, Mexico earthquake ($M_W = 8.1$). We use a multiple source represented by three point sources representing the subevents of Houston & Kanamori (1986) with assumed source durations of 10, 10 and 3 s and seismic moments of 5.8×10^{27}, 4.0×10^{27} and 1.3×10^{27} dyne cm, which are placed on a node 16 km below the free surface. For the last of the multiple sources we have assigned a much shorter source duration than that 10 s originally proposed by Houston & Kanamori (1986), since a number of studies indicate an anomalous wave radiation with periods close to 3 s for the last event (e.g. Singh *et al.* 1988, 1990; Campillo *et al.* 1989). As we have seen in the previous experiments, the presence of short-period radiation from the source is very important for the generation of a strong *Lg* wave.

Fig. 15 shows snapshots of the surface ground motion produced by the three subevents of the 1985 Michoacan earthquake. In the first frame (40 s), the spreading *P* and *S* wave

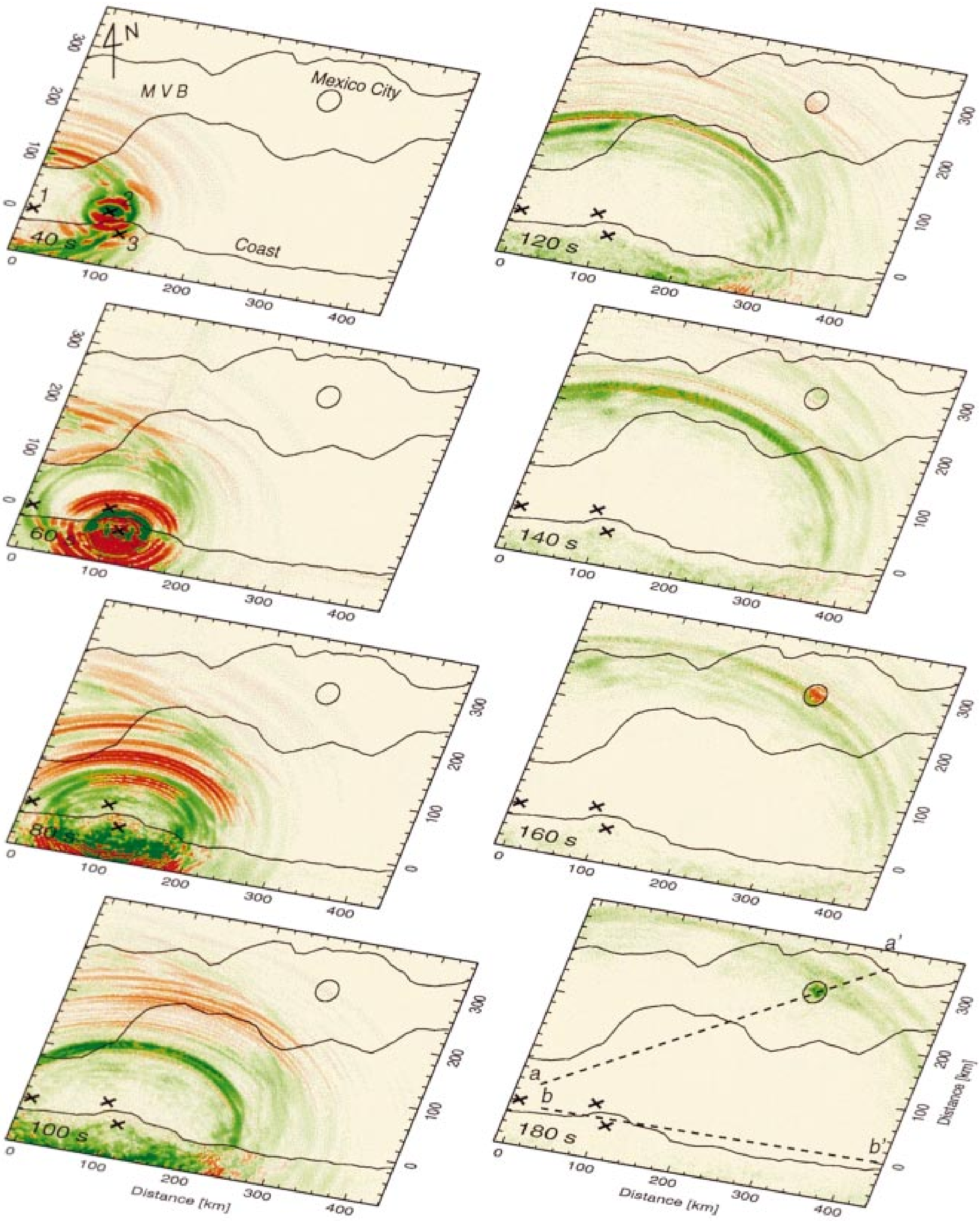

Figure 15. Snapshot of seismic wave propagation for the 1985 Michoacan earthquake calculated by the 3-D pseudospectral modelling illustrating the *P* and *S* waves at the surface. Three subevents (1–3) for the earthquake are shown in the bottom left corners. Distance is measured from the epicentre of the first event.

GJI000 16/11/98 13:23:08 3B2 version 5.20
The Charlesworth Group, Huddersfield 01484 517077

fronts from the first event and the radiation of seismic waves from the second event, which starts 21 s after the first, are seen. The 60 s snapshot shows the interaction of the *S* waves from the two subevents, which helps to enhance the *Sn*-wave amplitude propagating in the Mexican mainland and travelling towards Mexico City.

The third event starts 47 s after the first event and is responsible for producing large *Lg* waves (100 s frame). As the *Lg* waves propagate inland away from the source, the separation of a number of multiple *S* reflections within the crustal waveguide occurs, giving rise to a long tail on disturbances (120, 140 and 160 s). The *Lg* wave entering the basin of Mexico City is strongly enhanced by *Lg*-to-*P* conversions (160 s) and strong amplification in the sediment in the basin (180 s), which produce large and long oscillations of ground shaking in the basin.

We extract synthetic seismograms for two lines, an inland line (a–a′, Fig. 15) and a coastal line (b–b′). In the seismograms in Fig. 16, it is seen that at Mexico City there is a very long duration of ground oscillation associated with *S* waves.

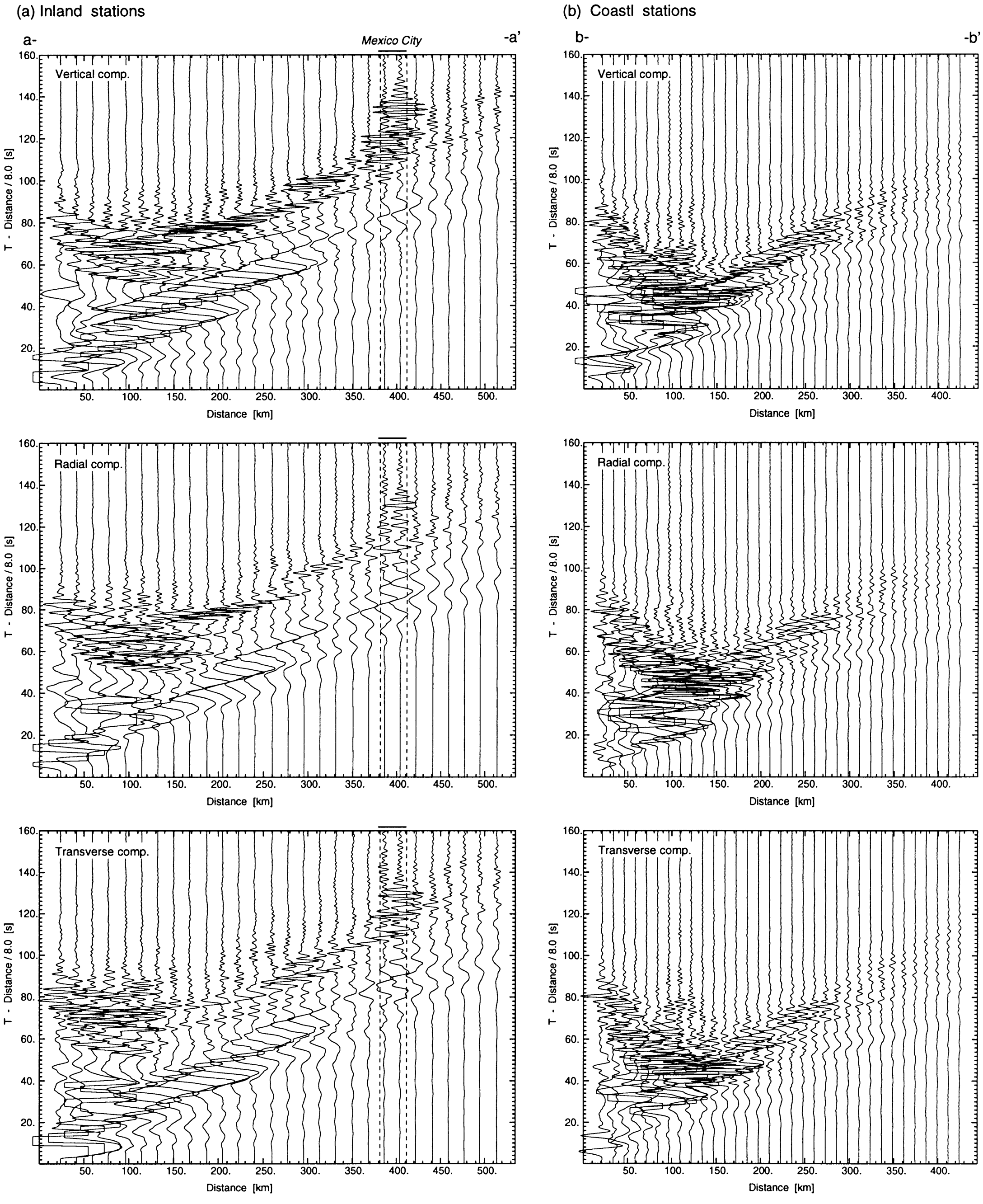

Figure 16. Synthetic velocity seismograms for vertical, radial and transverse components of the 1985 Michoacan earthquake for (a) inland stations (a–a′ in Fig. 15) and (b) coastal stations (b–b′ in Fig. 15). Distance is measured from the epicentre of the first event. Large phases are clipped.

GJI000 16/11/98 13:23:09 3B2 version 5.20
The Charlesworth Group, Huddersfield 01484 517077

From the arrival of the *Sn* wave radiated from the first event through the long coda of the *Lg* wave produced by the short-period waves from the third event, the *S* motion lasts for over 120 s. The strong motion at Mexico City shows a nearly monochromatic beating pattern of long and large ground oscillations, as seen during the damaging earthquake (see e.g. Singh *et al.* 1988, Fig. 3).

As we have seen in the synthetic seismograms for the 1995 Copala event, the dominance of *Lg* waves at regional distances is not seen in the coastal station records. There is a large amplitude maximum around 150 km from the epicentre produced by wide-angle *SmS* reflections from the Moho; the amplitude then decays suddenly at larger distances.

Fig. 17 shows the simulated peak ground velocity motion for horizontal and vertical motion for the 1985 Michoacan earthquake. There are a set of enhanced amplitude bands produced by the third event superposed on a broad amplified zone associated with the longer-period radiation from the first two events. We also confirm the presence of strong ground motion in Mexico City for both vertical and radial motion produced by amplification of the large incident waves impinging on the basin. It was very unfortunate for Mexico City during the great 1985 earthquake that enormously strong *S*-wave radiation with periods of 2–3 s was produced by the shallower subevent. These periods corresponded to a resonance in the basin of Mexico City and there was very efficient transport of *S*-wave energy within the crustal waveguide for the significant distance from the coast to Mexico City.

7 DISCUSSION AND CONCLUSIONS

The *Lg* phase is normally a dominant feature in the seismic wavefield at regional distances for all source types and depths in the upper crust. Since the *Lg* wave is built up from a number of multiple free-surface reflections of *S* waves within the crustal waveguide, the propagation character of the *Lg* wave is very sensitive to lateral variations in the crustal waveguide such as are produced by the subduction of oceanic crust below the continental material of western Mexico.

Numerical modelling of seismic wave propagation in 2-D and 3-D heterogeneous crustal models using both snapshots and synthetic seismograms has provided direct insight into the nature of the regional phases in the complex crustal waveguide. Using numerical simulations for a number of crustal models we have shown that the subducted plate acts to guide *S*-wave energy very efficiently into the crust. This near-source effect is promoted by the structure of the subducted plate with lower-velocity oceanic basalt with a strong velocity contrast to the high-velocity oceanic lithosphere beneath. The effective radiation characteristics produce large *Sn* and *Lg* arrivals on inland paths beyond 200 km from the epicentre.

Near-surface topography on the low-velocity surficial layer can also strongly enhance the *Lg* amplitude and the length of the wave train by scattering and *P* conversions. The large, long-duration input motion into the soft sediments below Mexico City helps to produce significant amplification in the wave motion, thus the anomalously large, long-duration ground shaking observed in Mexico City during damaging earthquakes arises from the combination of a number of factors: the characteristics of the source and its surroundings, the influence of the long propagation path and the local site conditions.

We have been able to reproduce the propagation of seismic waves in Mexico excited by subduction zone earthquakes using a realistic 3-D structural model. The recorded waves are strongly influenced by the heterogeneity in the crustal waveguide introduced by the subduction of the Cocos Plate and the near-surface geology of low-velocity rocks of the Mexican Volcanic Belt. Even though we were unable to include the very low-velocity surficial layer in the lake-bed zone of Mexico City in the 3-D simulation model, we successfully demonstrated the amplification and long duration of seismic waves observed in the basin.

The local amplification due to the soft sediments just below the free surface is responsible for much of the very strong ground motion during the damaging earthquake in Mexico City. This amplification has been the target of studies directed at estimating site responses for assessing hazard from future subduction zone events. The results of the present paper suggests that a comprehensive study of the source characteristics, wave propagation path and site amplification effects should also be undertaken when evaluating the strong ground motion from regional earthquakes.

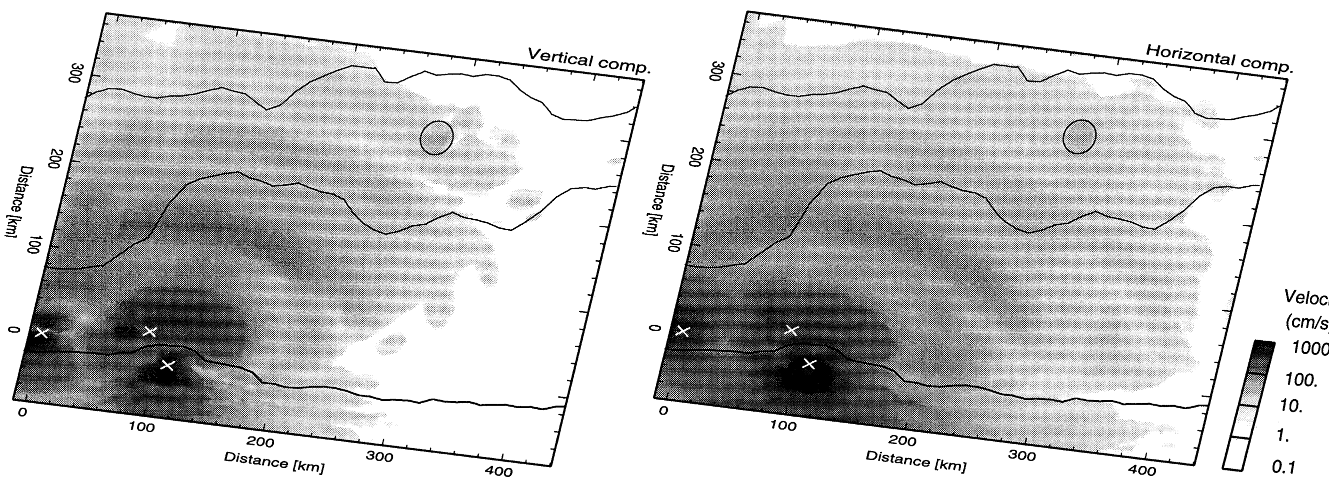

Figure 17. Maximum ground velocity distribution for the vertical (left) and the horizontal component (right) (vector mean of two components) derived from the 3-D simulation of the 1985 Michoacan earthquake.

GJI000 16/11/98 13:23:10 3B2 version 5.20
The Charlesworth Group, Huddersfield 01484 517077

ACKNOWLEDGMENTS

The authors wish to express their gratitude to Prof. F. J. Sánchez-Sesma, Dr. R. Quaas and Dr. L. Alcantara (Instituto de Ingeniería, Universidad Nacional Autonoma de Mexico, Ciudad Universitaria), Prof. J. G. Anderson (Seismological Laboratory and Department of Geological Sciences, Mackay School of Mines, University of Nevada, Reno) and Dr. J. Aguirre (Disaster Prevention Research Institute, Kyoto University) who kindly sent us strong ground motion data. TF is also grateful to Prof. K. Irikura (DPRI, Kyoto University) for providing important suggestions on seismic wave propagation in Mexico. TF acknowledges support from the Japan Ministry of Education, Culture and Sciences for research abroad and a Visiting Fellowship from the Research School of Earth Sciences, the Australian National University. Constructive comments from an anonymous reviewer are appreciated.

REFERENCES

Anderson, J. *et al.*, 1995. The Copala, Guerrero, Mexico earthquake of September 14, 1995 ($M_W = 7.4$): a preliminary report, *Seism. Res. Lett.*, **66,** 11–39.

Anderson, J.G. & Quaas, R., 1988. The Mexico earthquake of September 19, 1985—effect of magnitude on the character of strong ground motion: an example from the Guerrero, Mexico strong motion network, *Earthq. Spectra,* **4,** 635–651.

Anderson, J.G., Bodin, P., Brune, J.N., Prince, J., Singh, S.K., Quaas, R. & Onate, M., 1986. Strong ground motion from the Michoacan, Mexico, earthquake, *Science,* **233,** 1043–1049.

Bard, P.-Y. & Chávez-García, F.J., 1993. On the decoupling of surficial sediments from surrounding geology at Mexico City, *Bull. seism. Soc. Am.,* **83,** 1979–1991.

Bard, P.-Y., Campillo, M., Chávez-García, F.J. & Sánchez-Sesma, F., 1988. The Mexico earthquake of September 19, 1985—a theoretical investigation of large- and small-scale amplification effects in the Mexico City valley, *Earthq. Spectra,* **4,** 609–633.

Barker, J.S., Campillo, M., Sánchez-Sesma, F.J., Jongmans, D. & Singh, S.K., 1996. Analysis of wave propagation in the Valley of Mexico from a dense array of seismometers, *Bull. seism. Soc. Am.,* **86,** 1667–1680.

Baumgardt, D.R., 1990. Investigation of teleseismic *Lg* blockage and scattering using regional arrays, *Bull. seism. Soc. Am.,* **80,** 2261–2281.

Blandford, R.R., 1996. Regional seismic event discrimination, in *Monitoring a Comprehensive Test Ban Treaty,* pp. 689–719, eds Husebye, E.S. & Dainty, A.M., Kluwer Academic, Dordrecht.

Bowman, R. & Kennett, B.L.N., 1991. Propagation of *Lg* waves in the North Australian craton: influence of crustal velocity gradients, *Bull. seism. Soc. Am.,* **81,** 592–610.

Campillo, M., 1987. *Lg* wave propagation in laterally varying crust and the distribution of the apparent quality factor in central France, *J. geophys. Res.,* **92,** 12 604–12 614.

Campillo, M., Bard, P.-Y., Nicollin, F. & Sánchez-Sesma, F., 1988. The Mexico earthquake of September 19, 1985—the incident wavefield in Mexico City during the great Michoacán earthquake and its interaction with the deep basin, *Earthq. Spectra,* **4,** 591–608.

Campillo, M., Gariel, J.C., Aki, K. & Sánchez-Sesma, F.J., 1989. Destructive strong ground motion in Mexico City: source, path and site effects during great 1985 Michoacán Earthquake, *Bull. seism. Soc. Am.,* **79,** 1718–1735.

Catchings, R.D., Kohler, W.M., 1996. Reflected seismic waves and their effect on strong shaking during the 1989 Loma Prieta, California, earthquake, *Bull. seism. Soc. Am.,* **86,** 1401–1416.

Cerjan, C., Kosloff, D., Kosloff, R. & Reshef, M., 1985. A non-reflecting boundary condition for discrete acoustic and elastic wave equations, *Geophysics,* **50,** 705–708.

Chávez-García, F.J. & Bard, P.-Y., 1993a. Gravity waves in Mexico City?—I. Gravity perturbed waves in anelastic solid, *Bull. seism. Soc. Am.,* **83,** 1637–1655.

Chávez-García, F.J. & Bard P.-Y., 1993b. Gravity waves in Mexico City?—II. Coupling between an anelastic solid and a fluid layer, *Bull. seism. Soc. Am.,* **83,** 1656–1675.

Chávez-García, F.J. & Bard P.-Y., 1994. Site effects in Mexico City eight years after the September 1985 Michoacan earthquakes, *Soil Dyn. Earthq. Eng.,* **13,** 229–247.

Chávez-García, F.J. & Bard P.-Y., 1995. Reply to comment on 'Comment on two articles on gravity waves by Chávez-García and Bard (1993a,b)' by C. Lomnitz, *Bull. seism. Soc. Am.,* **85,** 1272–1274.

Chávez-García, F.J., Ramos-Martínez, J. & Romero-Jiménez, E., 1995. Surface-wave dispersion analysis in Mexico City, *Bull. seism. Soc. Am.,* **85,** 1116–1126.

Cocco, M., Pacheco, J., Singh, S.K. & Courboulex, F., 1997. The Zihuatanejo, Mexico, earthquake of 1994 December 10 ($M = 6.6$): source characteristics and tectonic implications, *Geophys. J. Int.,* **131,** 135–145.

Daudt, C.R., Braile, L.W., Nowack, R.L. & Chiang, C.S., 1989. A comparison of finite-difference and Fourier method calculations of synthetic seismograms, *Bull seism. Soc. Am.,* **79,** 1210–1230.

Fäh, D., Suhadolc, P., Mueller, St. & Panza, G.F., 1994. A hybrid method for the estimation of ground motion in sedimentary basins: quantitative modeling for Mexico City, *Bull. seism. Soc. Am.,* **84,** 383–399.

Flores, J., Novaro, O. & Seligman, T.H., 1987. Possible resonance effect in the distribution of earthquake damage in Mexico City, *Nature,* **326,** 783–785.

Fornberg, B., 1987. The pseudospectral method: comparison with finite differences for the elastic wave equation, *Geophysics,* **52,** 483–501.

Furumura, T. & Kennett, B.L.N., 1997. On the nature of regional seismic phases—II. On the influence of structural barriers, *Geophys. J. Int.,* **129,** 221–234.

Furumura, T. & Takenaka, H., 1990. Theoretical seismograms by the pseudospectral method, *Proc. 83rd SEGJ Conference,* 13–18 (in Japanese).

Furumura, T. & Takenaka, H., 1996. 2.5-D modelling of elastic waves using the pseudospectral method, *Geophys. J. Int.,* **124,** 820–832.

Furumura, T., Takenaka, H. & Koketsu, K., 1996. Numerical 3-D modeling of seismic waves by the pseudospectral method, *Butsuri-Tansa (J. Soc. Expl. Geophys.),* **49,** 536–548 (in Japanese).

Furumura, T., Kennett, B.L.N. & Takenaka, H., 1998. Parallel 3-D pseudospectral simulation of seismic wave propagation, *Geophysics,* **63,** 279–288.

Gibson, R.L., Jr & Campillo, M, 1994. Numerical simulation of high- and low-frequency *Lg*-wave propagation, *Geophys. J. Int.,* **118,** 47–56.

Goldstein, P., Schultz, C. & Larsen, S., 1997. The influence of deep sedimentary basins, crustal thinning, attenuation, and topography on regional phases: selected examples from the Eastern Mediterranean and the Caspian Sea regions, *Proc. 19th Ann. Seism. Res. Symp. on CTBT,* 486–494.

Gregersen, S., 1984. *Lg*-wave propagation and crustal structure differences near Denmark and the North Sea, *Geophys. J. R. astr. Soc.,* **79,** 217–234.

Herrmann, R.B. & Kijko, A., 1983. Modeling some empirical vertical component *Lg* relations, *Bull. seism. Soc. Am.,* **73,** 157–171.

Houston, H. & Kanamori, H., 1986. Source characteristics of the 1985 Michoacan, Mexico earthquake at periods of 1 to 30 seconds, *Geophys. Res. Lett.,* **13,** 597–600.

Kawase, H. & Aki, K., 1989. A study on the response of a soft basin for incident *S, P,* and Rayleigh waves with special reference to the

GJI000 16/11/98 13:23:11 3B2 version 5.20
The Charlesworth Group, Huddersfield 01484 517077

long duration observed in Mexico City, *Bull. seism. Soc. Am.,* **79,** 1361–1382.

Kennett, B.L.N., 1989. On the nature of regional seismic phases—I. Phase representations for *Pn, Pg, Sn, Lg*, *Geophys, J. R. astr. Soc.,* **98,** 447–456.

Kennett, B.L.N, 1993. The distance dependence of regional phase discriminants, *Bull. seism. Soc. Am.,* **83,** 1155–1166.

Kennett, B.L.N. & Mykkeltveit, S., 1984. Guided wave propagation in laterally varying media—II. *Lg*-waves in north-western Europe, *Geophys, J. R. astr. Soc.,* **79,** 257–267.

Kosloff, D., Reshef, M., Loewenthal, D., 1984. Elastic wave calculation by the Fourier method, *Bull. seism. Soc. Am.,* **74,** 875–891.

Lomnitz, C., 1990. Mexico 1985: the case for gravity waves, *Geophys. J. Int.,* **102,** 569–572.

Lomnitz, C., 1995. Comments on two articles on gravity waves by Chávez-García and Bard (1993a,b), *Bull. seism. Soc. Am.,* **85,** 1271.

Mateos, J.L., Flores, J., Novaro, O., Alvarez-Tostado, J.M. & Seligman, T.H., 1993a. Generation of inhomogeneous P waves in a layered medium, *Tectonophysics,* **218,** 247–256.

Mateos, J.L., Flores, J., Novaro, O., Seligman, T.H., & Alvarez-Tostado, J.M., 1993b. Resonant response models for the Valley of Mexico—II. The trapping of horizontal *P* waves, *Geophys. J. Int.,* **113,** 449–462.

Nuttli, O., 1988. *Lg* magnitude and yield estimates for underground Novaya Zemlya nuclear explosions, *Bull. seism. Soc. Am.,* **78,** 873–884.

Olsen, K.H., Braile, L.W. & Stewart, J.N., 1983. Modeling short-period crustal phases ($\bar{\mathrm{P}}$, Lg) for long-range reflection profiles, *Phys. Earth planet. Inter.,* **31,** 334–347.

Ordaz, M. & Singh, S.K., 1992. Source spectra and spectral attenuation of seismic waves from Mexican earthquakes, and evidence of amplification in the hill zone of Mexico City, *Bull. seism. Soc. Am.,* **82,** 24–43.

Pardo, M. & Suárez, G., 1995. Shape of the subducted Rivera and Cocos plates in southern Mexico: seismic and tectonic implications, *J. geophys. Res.,* **100,** 12 357–12 373.

Pomeroy, P.W., Best, W.J. & McEvilly, T.J., 1982. Test ban treaty verification with regional data—a review, *Bull. seism. Soc. Am.,* **72,** S89–S129.

Press, F. & Ewing, M., 1952. Two slow surface waves across North America, *Bull. seism. Soc. Am.,* **42,** 219–228.

Quaas, R. *et al.,* 1996. Mexican strong motion database. An integrated system to compile accelerograph data from the past 35 years, *Proc. 11th World Conference on Earthquake Engineering,* Paper No. 1804.

Reshef, M., Kosloff, D., Edwards, M. & Hsiung, C., 1988. Three-dimensional elastic modeling by the Fourier method, *Geophysics,* **53,** 1184–1193.

Sánchez-Sesma, F.J. & Luzón, F., 1996. Can horizontal *P* waves be trapped and resonate in a shallow sedimentary basin?, *Geophys. J. Int.,* **124,** 209–214.

Sánchez-Sesma, F., Chávez-Pérez, S., Suárez, M., Bravo, M.A. & Pérez-Rocha, L.E., 1988. The Mexico earthquake of September 19, 1985—on the seismic response of the Valley of Mexico, *Earthq. Spectra,* **4,** 569–589.

Sánchez-Sesma, F.J., Pérez-Rocha, L.E. & Reinoso, E., 1993. Ground motion in Mexico City during the April 25, 1989, Guerrero earthquake, *Tectonophysics,* **218,** 127–140.

Seligman, T.H., Alvarez-Tostado, J.M., Mateos, J.L, Flores, J. & Novaro, O., 1989. Resonant response models for the Valley of Mexico—I. The elastic inclusion approach, *Geophys. J. Int.,* **99,** 789–799.

Shapiro, N.M., Campillo, M., Paul, A., Singh, S.K., Jongmans, D. & Sánchez-Sesma, F.J., 1997. Surface-wave propagation across the Mexican Volcanic Belt and the origin of the long-period seismic-wave amplification in the Valley of Mexico, *Geophys. J. Int.,* **128,** 151–166.

Singh, S.K. & Ordaz, M., 1993. On the origin of long coda observed in the lake-bed strong-motion records of Mexico City, *Bull. seism. Soc. Am.,* **83,** 1298–1306.

Singh, S.K. & Pardo, M., 1993. Geometry of the Benioff zone and state of stress in the overriding plate in Central Mexico, *Geophys. Res. Lett.,* **20,** 1483–1486.

Singh, S.K., Suárez, G. & Domínguez, T., 1985. The Oaxaca, Mexico, earthquake of 1931: lithospheric normal faulting in the subducted Cocos plate, *Nature,* **317,** 56–58.

Singh, S.K., Mena, E. & Castro, R., 1988. Some aspects of source characteristics of the 19 September 1985 Michoacan earthquake and ground motion amplification in and near Mexico City from strong motion data, *Bull. seism. Soc. Am.,* **78,** 451–477.

Singh, S.K., Mori, A., Mena, E., Krüger, F. & Kind, R., 1990. Evidence for anomalous body-wave radiation between 0.3 and 0.7 Hz from the 1985 September 19 Michoacan, Mexico earthquake, *Geophys. J. Int.,* **101,** 37–48.

Singh, S.K., Quaas, R., Ordaz, M., Mooser, F., Almora, D., Torres, M. & Vásquez, R., 1995. Is there truly a 'hard' rock site in the Valley of Mexico?, *Geophys. Res. Lett.,* **22,** 481–484.

Singh, S.K., Ordaz, M. & Pérez-Rocha, L.E., 1996. The great Mexican earthquake of 19 June 1858. Expected ground motions and damage in Mexico City from a similar future event, *Bull. seism. Soc. Am.,* **86,** 1655–1666.

Somerville, P. & Yoshimura, J., 1990. The influence of critical Moho reflections on strong ground motion recorded in San Francisco and Oakland during the 1989 Loma Prieta earthquake, *Geophys. Res. Lett.,* **17,** 1203–1206.

Suárez, G., Monfret, T., Wittlinger, G. & David, C., 1990. Geometry of subduction and depth of the seismogenic zone in the Guerrero gap, Mexico, 1990, *Nature,* **345,** 336–338.

Suter, M., Carrillo-Martínez, M. & Quintero-Legorreta, O., 1996. Macroseismic study of shallow earthquakes in the central and eastern parts of the trans-Mexican Volcanic belt, Mexico, *Bull. seism. Soc. Am.,* **86,** 1952–1963.

Valdes, C.M. *et al.,* 1986. Crustal structure of Oaxaca, Mexico, from seismic refraction measurements, *Bull. seism. Soc. Am.,* **76,** 547–563.

Yamamoto, J., Quintanar, L., Herrmann, R.B. & Fuentes, C., 1997. Lateral variation of Lg coda *Q* in southern Mexico, *Pure. appl. Geophys.,* **149,** 575–599.

Zang, T. & Lay, T., 1994. Analysis of short-period regional phase path effects associated with topography in Eurasia, *Bull. seism. Soc. Am.,* **84,** 119–132.

GJI000 16/11/98 13:23:13 3B2 version 5.20
The Charlesworth Group, Huddersfield 01484 517077